Tectonics®

RESEARCH ARTICLE
10.1029/2025TC008859

**Special Collection:**
Fold-and-Thrust Belts: Evolution and Dynamics at All Spatiotemporal Scales

# Interaction Between Transverse and Rift Faults During the Initiation of Orogenic Extension: The Case of Sant'Anna Pelago (Northern Apennines, Italy)

**S. Lenci[1], D. Keir[1,2], G. Molli[3], C. Pagli[3], P. Vannucchi[1], and C. Del Ventisette[1]**

[1]Department of Earth Sciences, University of Florence, Florence, Italy, [2]School of Ocean and Earth Science, University of Southampton, Southampton, UK, [3]Department of Earth Sciences, University of Pisa, Pisa, Italy

**Abstract** Sant'Anna Pelago is located near the extensional front of the Northern Apennines (Italy) between Modena and Lucca, an area characterized by multiple lateral steps of the NW-SE striking tectonic system and orographic divide. The region is affected by significant instrumental seismicity with over a thousand recorded events ($0.5 < M < 4.8$) from 2006 to 2024, and few $4.13 < Mw < 4.33$ historical earthquakes. Nevertheless, it is not clear what are the geometries and kinematics of the faults, nor which are seismogenic, and as a result we have few constraints on how extensional basins initiate and link across their lateral steps. In this study we performed absolute and relative relocation of earthquakes and focal mechanism computation to analyze the most significant seismic sequences. We calculated Coulomb stress changes from the 2013 $Mw = 4.8$ strike-slip mainshock that occurred on a fault transverse to the Apennines and show that it caused the 2013 aftershock sequence on an overlying, NW-SE striking normal fault. Most of the other sequences occurred on a nearby system of steep, en echelon normal faults. Structural field observations support the existence of a major strike-slip transverse deformation zone extending to the Sant'Anna Pelago area. Our results show that extensional and transverse strike-slip faults can be active synchronously and closely interact through mechanisms such as stress triggering.

**Key Points:**

- Local extensional front features coeval deep transverse strike-slip faults and shallower normal faults with near-orthogonal directions
- The slip of a deep transverse fault triggered a major orthogonal rift fault at shallow levels
- Early extensional transverse faults superimpose on a contractional step zone within the thrust-and-fold belt

**Supporting Information:**

Supporting Information may be found in the online version of this article.

**Correspondence to:**
S. Lenci,
simone.lenci@unifi.it

**Citation:**
Lenci, S., Keir, D., Molli, G., Pagli, C., Vannucchi, P., & Del Ventisette, C. (2025). Interaction between transverse and rift faults during the initiation of orogenic extension: The case of Sant'Anna Pelago (Northern Apennines, Italy). *Tectonics*, *44*, e2025TC008859. https://doi.org/10.1029/2025TC008859

Received 31 JAN 2025
Accepted 29 AUG 2025

**Author Contributions:**
**Conceptualization:** S. Lenci, D. Keir, G. Molli, C. Pagli
**Data curation:** S. Lenci
**Formal analysis:** S. Lenci
**Investigation:** S. Lenci
**Methodology:** S. Lenci, D. Keir, C. Pagli
**Software:** S. Lenci, C. Pagli
**Supervision:** D. Keir, G. Molli, C. Pagli, P. Vannucchi, C. Del Ventisette
**Visualization:** S. Lenci
**Writing – original draft:** S. Lenci, D. Keir



## 1. Introduction

Extending orogens and rifts exhibit complex three-dimensional fault patterns, arising from the long-term history of fault nucleation, propagation and interaction (Fossen & Rotevatn, 2016; Gawthorpe & Leeder, 2000; Morley, 2010). Some faults have unexpected orientations that do not follow Andersonian fault theory. These commonly form due to local re-orientation of the tectonic stress, or by re-activating faults inherited from prior tectonic events (Dawson et al., 2018; Maestrelli et al., 2020; McClay, 1995; Morley, 2010, 2017; Zwaan & Schreurs, 2017), and can strike at high angles respect to the evolving mountain belt or rift axis (Chorowicz, 1989; Corti et al., 2022; Illies, 1972; Laõ-Dávila et al., 2015; Lezzar et al., 2002; Martin et al., 1993; Morley et al., 2007; Muirhead & Kattenhorn, 2018). However, in most settings it is unclear what the kinematics of these faults are, and how they influence fault network and tectonic evolution of a region. With the increase in passive seismic data in many regions globally, it is now becoming increasingly possible to image the subsurface shape and kinematics of complex fault networks.

The Northern Apennines, in Italy, is a mountain chain characterized by contemporaneous active slow-rate contraction in the foreland to the east (Basili & Barba, 2007; Benedetti et al., 2000; Boccaletti et al., 2011; Burrato et al., 2003; Picotti & Pazzaglia, 2008; Wilson et al., 2009) and extension in the internal domain in the west (Bennett et al., 2012; Carmignani & Kligfield, 1990; Frepoli & Amato, 1997; Ghisetti & Vezzani, 2002; Molli et al., 2021). Both extensional and contractional fronts migrate NE-ward due to chain-scale counter-clockwise rotation (Bennett et al., 2012; Le Breton et al., 2017; Mantovani et al., 2015). At a local scale deformation is accommodated on a multitude of segmented structures which have prominent lateral steps at all-scales. In the internal domain the lateral steps are mainly expressed as a series of left-stepping, en echelon and overlapping basins of NW-SE (Apenninic) orientation (Figures 1 and 2). Previous studies have hypothesized that steps originated from structural lineaments oriented almost perpendicular or "transverse" (sensu Ben-Avraham & Ten Brink, 1989) to the chain front. These lineaments are believed to control large scale segmentation of major fault systems and basin development (Brogi et al., 2020; Elter et al., 2012; Molli et al., 2021; Pascucci et al., 2007; Sorgi et al., 1998). However, the faults underlying these transverse lineaments have rarely been observed, and the style and kinematics of the expected lateral shearing associated with them is unclear, as is their seismogenic

**Writing – review & editing:** D. Keir, G. Molli, P. Vannucchi

potential. As a result, the existence and kinematics of transverse faults and their interaction in space and time with the morphologically clearer Apenninic faults are highly debated.

The area situated near the Northern Apennines orographic divide between Modena and Lucca (Figures 1a and 2), where the tectonically active basins in the internal domain are arranged in an en echelon pattern (Figure 1a), provides an ideal context for studying these topics. This setting motivated our focus on the Sant'Anna Pelago area, where over the past ∼15 years significant instrumental seismicity has been recorded, characterized by moderate to low-magnitude earthquakes. Notable events include $Mw = 4.13$ (1909), $Mw = 4.28$ (1988), $Mw = 4.33$ (1997) (Locati et al., 2022; Rovida et al., 2022). Here, in 2013, the National Institute of Geophysics and Volcanology (INGV) catalog (ISIDe Working Group, 2007) reports a $Mw = 4.8$ mainshock at around 20 km depth, with the focal mechanism showing almost pure strike-slip motion, and then followed by a dense seismic sequence. The map distribution of the INGV locations shows a NW-SE elongated cloud of seismicity, broadly parallel to the local Apennine front. However, the catalog locations lack the spatial definition required to associate the mainshock and aftershocks to specific faults, and a focal mechanism has only been computed for the mainshock. In addition, mapped faults show no evidence for pure strike-slip motion on near vertical Apenninic structures (Martelli et al., 2016a, 2016b), which generally show only little lateral slip components (Molli et al., 2021). The Italian database of seismogenic structures (DISS Working Group, 2021) does not include any seismic sources across the orographic divide (Figure 2), and the catalog of capable faults (ITHACA Working Group, 2019) doesn't report any active capable fault in the area. As such, it is both unclear what are the subsurface geometry and kinematics of faults during the sequence, and how this relates to the mapped expression of faults at the surface. Identifying the arrangement the overall architecture of seismogenic faults in this region is crucial for anticipating where earthquakes might occur in the future.

To address these questions, we use seismological and structural analysis in the Sant'Anna Pelago area and its surroundings. We use double difference (DD) earthquake relocations to create a high-resolution seismicity catalog spanning 2006–2023. We use the new catalog to identify the location, the extent and the geometries of individual seismogenic faults and computed focal mechanisms to determine their kinematics. The result shows evidence for complex fault network of NW-SE striking normal faults above a NE striking strike-slip fault that slipped during the 2013 main-shock. We use Coulomb stress change (CSC) modeling to evaluate to what extent the various seismic sequences were triggered by the mainshock. Finally, we interpret the results from the seismicity and stress change models considering new kinematic data and reinterpreted existing structural maps of the region.

## 2. Geologic and Seismotectonic Setting

### 2.1. Northern Apennines Tectonic Evolution

The Northern Apennines are a northeast-verging thrust-and-fold belt formed from the polyphase deformation of a stack of Adria-derived continental units and remnants of a former accretionary wedge (Carmignani & Kligfield, 1990; Doglioni et al., 1998; Elter, 1975; Jolivet et al., 1998; Molli, 2008; Remitti et al., 2007) (Figure 3). Since the Neogene (∼23 Ma), deformation has occurred through coeval slow-rate contraction in the foreland to the NE, and extension in the internal domains to the SW, with both fronts continuously migrating northeast-ward through counter-clockwise rotation (Boccaletti et al., 1971; Caricchi et al., 2014; Doglioni et al., 1998; Jolivet & Faccenna, 2000; Le Breton et al., 2017; Molli et al., 2021), driven by the NE-ward rollback of the subducting Adriatic plate (Doglioni, 1991; Faccenna et al., 2014; Le Breton et al., 2017; Meletti et al., 2000; Serpelloni et al., 2005). Shortening involved the north eastward sequential incorporation of proximal to distal continental units beneath the advancing forearc, accompanied by discontinuous out-of-sequence thrusting (Figure 3) (Clemenzi et al., 2014; Fazzuoli et al., 1994; Molli et al., 2018; Plesi et al., 1998; Reutter et al., 1983; Vannucchi et al., 2008; Vescovi, 2005). Multiple top-to-southeast and top-to-northwest, highly oblique structures and ramps allowed lateral transfer of shortening between thrust sheets.

Since the Pliocene (∼5 Ma), the internal Northern Apennines have experienced extension by high-angle faults (HAFs), which now mainly bound westward oldening intramontane basins of Plio-Pleistocene formation or reactivation. Toward the west the degree of overprinting of compressional fabrics and thrust related morphology by the HAFs also increases (Molli et al., 2021; Pascucci et al., 2007). The westward increase in extension has resulted in across-chain variations in crustal thickness, from <20 km off-shore in the Tyrrhenian sea and

10.1029/2025TC008859

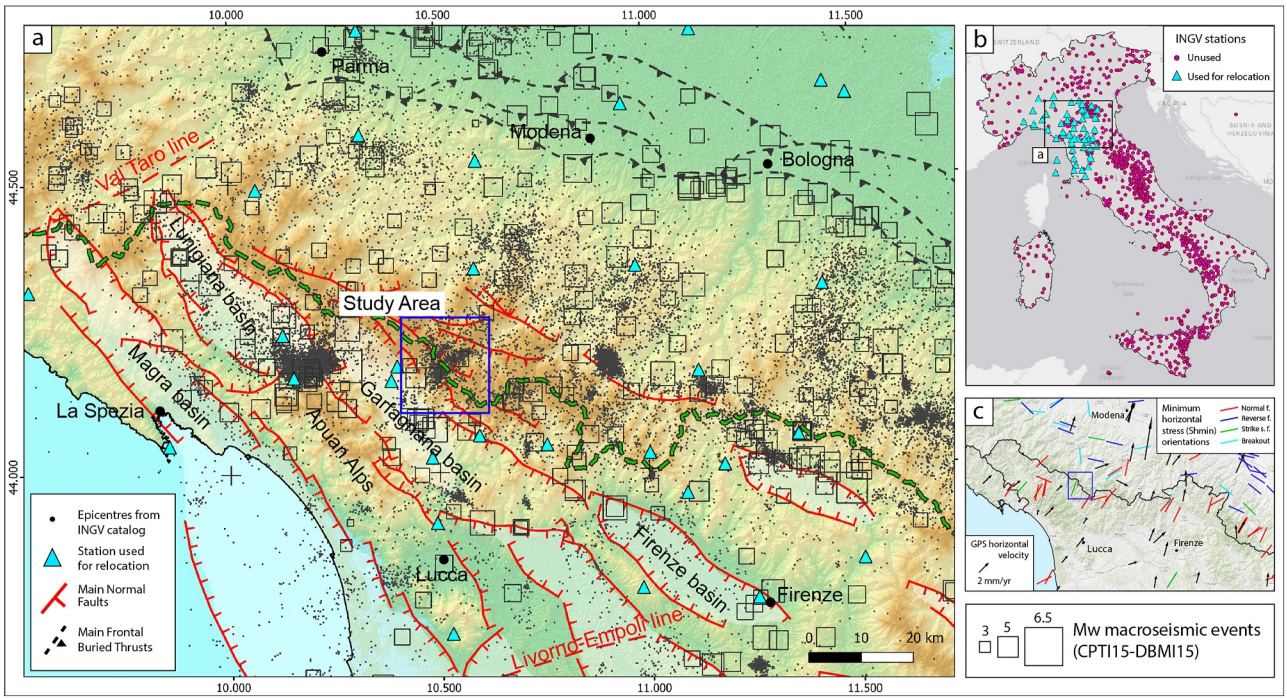


**Figure 1.** (a) Seismotectonic map of the Northern Apennines reporting recorded earthquakes distribution (National Institute of Geophysics and Volcanology (INGV) catalog), historical earthquakes (Locati et al., 2022; Rovida et al., 2022), major high-angle faults and foreland thrusts (Bigi et al., 1990; Martelli et al., 2016b; Molli et al., 2021). The blue frame refers to study area of Figure 5a. (b) Map of Italy with INGV stations network (in cyan those used for relocation). Panel (c) map with Shmin directions (Mariucci & Montone, 2024) and GPS velocities (Bennett et al., 2012).

increasing progressively to ~50 km near the orographic divide (Dannowski et al., 2020; Di Stefano & Ciaccio, 2014; Ferretti et al., 2002; Li et al., 2007; Mele & Sandvol, 2003; Piana Agostinetti & Amato, 2009).

Extension has also led to a significant along-chain variations in the amount of stretching, resulting in a SE increase in width of extended crust and the formation of left-stepping, en echelon and overlapping basins (Molli et al., 2021). Controls on the segmentation of the basins and how deformation occurs in basin steps is not entirely clear but have previously been associated at a range of scales to NE–SW striking medium to high angle transverse (oriented highly oblique to perpendicular to the orogen) faults. These faults are largely inferred indirectly from geomorphological, geophysical, and tectono-stratigraphic data, and not often directly observable, except where they are exhumed (Cortopassi et al., 2006; Molli et al., 2015) or they cut and offset recent surficial Quaternary markers (Brogi et al., 2020, 2024; Cantini et al., 2001). The transverse structures have been interpreted to cover a wide range of fault types and kinematics. These include transfer faults, thrust sheet lateral ramps, pure dextral and sinistral strike-to oblique-slip faults, pure normal or hybrid faults (Coltorti et al., 1996; Dramis et al., 1991; Ghelardoni, 1965; Locardi, 1988; Molli et al., 2018; Pascucci et al., 2006, 2007). Some of these faults may have functioned as different types at various stages of the orogen's evolution (Liotta, 1991; Tavarnelli et al., 2004), reflecting their role as persistent structural weaknesses (Liotta, 1991; Morley, 2010; Pizzi & Galadini, 2009). Although some studies have linked low to medium-high magnitude earthquake sequences to transverse structures (Albarello et al., 2005; Bonini et al., 2016; Brogi et al., 2020; Buonasorte et al., 1987; Kaerger et al., 2024; Liotta, 1991; Mirabella et al., 2022; Molli et al., 2016; Pezzo et al., 2014; Stramondo et al., 2014; Vannoli et al., 2015), seismicity constraints are limited, and the true seismological potential largely remains unknown.

The area of Sant'Anna Pelago, located at the Apennine orographic divide, exhibits well documented elements from both the contractional and extensional phases. Main elements include large-scale asymmetric thrust sheets and frontal folds resulting from out-of-sequence shortening (Figure 3). Additionally, differential shortening has led to a significant lateral offset of the unit fronts, associated with highly oblique to near-transverse ramps. The main regional active HAFs in the area (Conti et al., 2020; Martelli et al., 2016a, 2016b; Molli et al., 2021) are between the western flank of Garfagnana basin and the frontal fold forelimb of the external unit to the east (Figures 2 and 3). The back-limb flats of the major frontal folds are characterized by SW dipping normal faults,

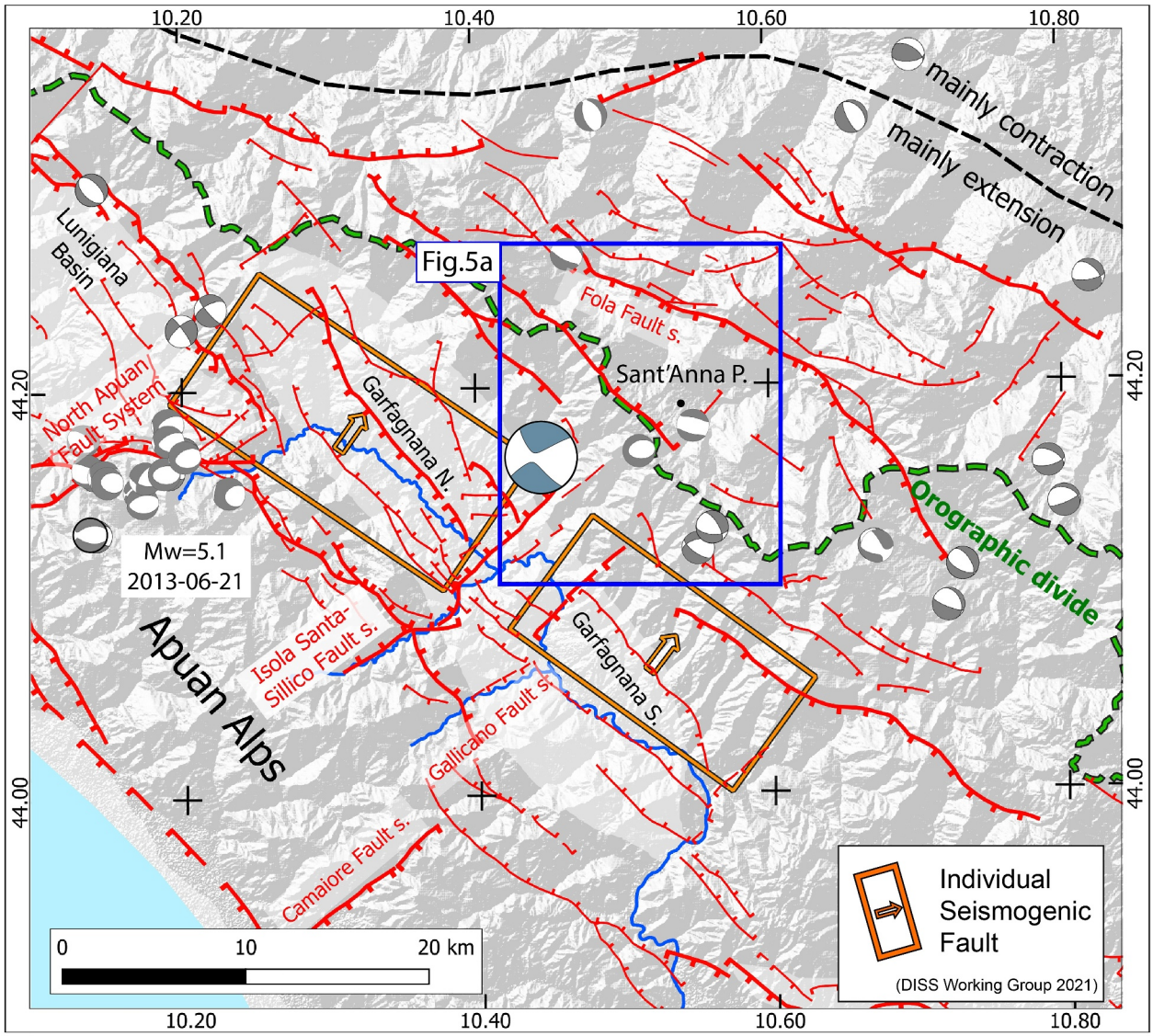


**Figure 2.** Tectonic sketch of the northern tip of Apennines rift with major transverse high-angle faults traces (from Conti et al., 2020; Martelli et al., 2016b; Molli et al., 2021), location of the seismogenic faults (Diss Working Group 2021) and focal mechanisms (Martelli et al., 2016b; Scognamiglio et al., 2006).

while NE dipping HAFs are on their steep forelimbs. NE-dipping normal faults adjust their orientations to align with the major lateral and frontal changes in the thrust sheet fronts, commonly showing curved NW-SE to E-W orientations. Major fault systems are shown in Figure 2. Sant'Anna Pelago lies in an asymmetric graben west of the SW-dipping Fola master fault system (Balocchi, 2020; Martelli et al., 2016a, Martelli et al., 2016b; Plesi et al., 2002a, 2002b), which is part of a ~25 km long regional fault systems with remarkable morpho-structural evidence.

Transverse faults also exist in the area (Figure 2). In mid-Garfagnana, a transversal morphological high is bounded by two major steep hybrid transverse systems, that is NW dipping Isola Santa-Sillico fault system (ISSF), which cut Pleistocene-Holocene fluvial deposits, and the SE-dipping Gallicano fault (Martelli et al., 2016a, 2016b; Molli et al., 2021). Some minor transverse faults include the transverse Sant'Anna fault, steeply dipping to the NW (Balocchi, 2020; Puccinelli et al., 2016a, 2016b).

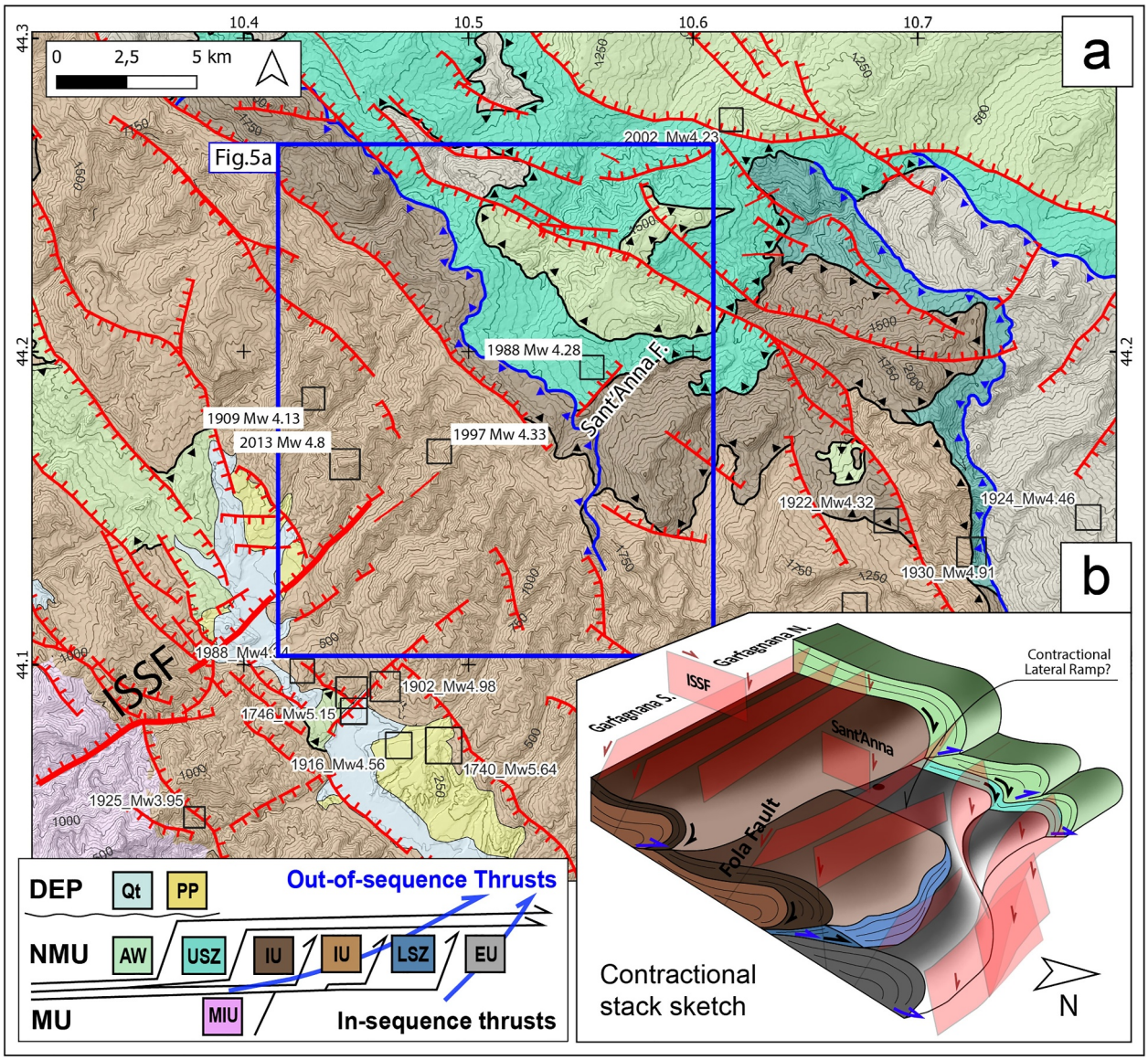


**Figure 3.** (a) Schematic geological map around the study area, with traces of the main contractional frontal ramps (black). Empty squares are historical $M > 4$ earthquakes (Rovida et al., 2022). At the bottom, simplified tectonic relations from the contractional history are shown. DEP = Neogene deposits; Qt = Quaternaty deposits; PP = Plio-Pleistocene deposits; NMU = Non-metamorphic units; AW = Accretionary wedge units; USZ; Upper shear zone, LSZ; Lower shear zone, IU = Internal units; EU = External units; MU = Metamorphic internal units. (b) 3D sketch of the pre-high-angle faults (HAFs) state of the contractional stack and future locations of HAFs in transparent.

### 2.2. Regional Seismicity

The Northern Apennines is a slow-deforming region, characterized by ~1–4 mm/yr horizontal velocity (Bennett et al., 2012; Cenni et al., 2013; Molli et al., 2021; Serpelloni et al., 2016, 2022). Present-day crustal motions and several geophysical studies on regional seismicity (Di Stefano & Ciaccio, 2014; Di Stefano et al., 2009, 2011; Ferretti et al., 2002; Li et al., 2007; Mele & Sandvol, 2003; Piana Agostinetti & Amato, 2009) show a wide region of extension, located along and mostly west of the main orographic divide, where minimum stress axis σ3 is ~NE-SW-oriented (Chiarabba et al., 2005; Martelli et al., 2016a, 2016b; Pondrelli et al., 2006).

Due to very low horizontal strain rates, and limited seismic network coverage until 2005 (Saccorotti et al., 2022), how deformation is distributed remains poorly understood. Figure 1a reports all instrumental earthquakes (ISIDe Working Group, 2007) and $M > 4$ historical earthquakes from the national catalog (Locati et al., 2022). The

internal domain exhibits sparse, weak, and relatively shallow (3–10 km) instrumental seismicity and lacks strong historical earthquakes (only a few $Mw > 4.0$). In contrast, most of the instrumental and historical seismicity is predominantly located along an elevated region comprising the outermost intramontane basins and the areas near the orographic divide. These events tend to occur in moderate to deep, dense clusters within the thicker crust, and have caused severe damage. Notable events include those in 1481 ($Ms = 5.9$), 1834 ($Ms = 5.6$), and 1837 ($Ms = 6.4$) in Lunigiana (Eva et al., 2025), and in 1740 ($Mw = 5.6$), 1746 ($Mw = 5.0$), 1902 ($Mw = 4.9$), 1920 ($Ms = 6.5$) and 1939 ($Mw = 4.9$) in Garfagnana (Figure 1a). More recently in 2013 the region experienced a significant sequence associated with a $Mw = 4.8$ mainshock in mid-Garfagnana (the focus of this study) and a $Mw = 5.1$ mainshock in southern Lunigiana (Figure 2).

Most focal mechanisms along the orographic divide and surrounding areas exhibit almost pure or slightly oblique normal kinematics with broadly ESE and SE Apenninic oriented nodal planes. A few mechanisms, such as 2013 mid-Garfagnana mainshock and Lunigiana main events, show highly oblique oriented (E-W) to transverse (SW-NE) nodal planes and normal-oblique to pure strike-slip motion (Figure 2).

Despite the region shows significant activity, only two composite seismogenic source are recognized in the national database (DISS Working Group, 2021), related to fault systems in the Lunigiana and Garfagnana basins. The latter is further subdivided into distinct Garfagnana North and Garfagnana South segments (Figure 2), characterized by NE dipping master faults, with the 2013 mainshock broadly centered between them. Three additional significant historical earthquakes, the 1909 ($Mw = 4.13$), 1988 ($Mw = 4.28$, ~20 km), and 1997 ($Mw = 4.33$, ~16 km) events, have been identified near the Sant'Anna area (Rovida et al., 2022), NE of the 2013 mainshock (Figure 3a).

## 3. Seismological and Structural Analysis

### 3.1. Data

The study area is monitored by the Italian Seismic Network (ISN, Istituto Nazionale di Geofisica e Vulcanologia, 2005). For the earthquake locations we used a phase-arrival data set from the publicly available INGV catalog (ISIDe Working Group, 2007). We used P- and S-wave arrival times from 1185 ML > 0.5 earthquakes, located within box of corners (44.107 N–10.438 E, 44.252 N–10.620 E) and recorded by 56 evenly distributed permanent stations within 150 km radius operating during 2006-01 to 2023-12 (Figure 1b). From 2013, the ISN offered dense station distribution, optimal azimuthal coverage and small inter-distance between instruments around the study area, resulting in low magnitude completeness.

Waveforms of earthquakes with $M > 2.5$ were downloaded from EIDA Data Archive (Danecek et al., 2021) to compute focal mechanisms. Regional data of fault traces were acquired from the updated map of active faults in Molli et al. (2021), and from the seismotectonic map of Emilia Romagna (Martelli et al., 2016a, 2016b).

### 3.2. Methods

#### 3.2.1. Absolute Locations

The P- and S-waves arrival times were used to perform our own absolute location of earthquakes with NonLinLoc (Lomax et al., 2014). NonLinLoc (NLL) uses a non-linear, probabilistic approach and provides a comprehensive estimate of the location uncertainties with "a posteriori" probability density function created by solving the inversion problem formulation proposed by Tarantola and Valette (1982). Earthquake location was performed using a local 1D velocity model (Figure S1 in Supporting Information S1) from the national tomographic P- and S-wave velocity model of Di Stefano and Ciaccio (2014). We adopted a grid of 1 km cubic cells, assuming uniform slowness inside each cell. The minimum number of phases to locate an event was set to 4. The processing resulted in 1,041 located events (Figure 4d).

#### 3.2.2. - Relative Relocation

We then refined earthquake location with relative DD relocation (Waldhauser & Ellsworth, 2000) using the *catalog* differential arrival times with HypoDD. Relocations using the DD algorithm are far less sensitive to the use of simplified 1D velocity models to represent complex crustal structures, compared to absolute location methods (Waldhauser & Ellsworth, 2000). The DD method minimizes the differential arrival times between

10.1029/2025TC008859

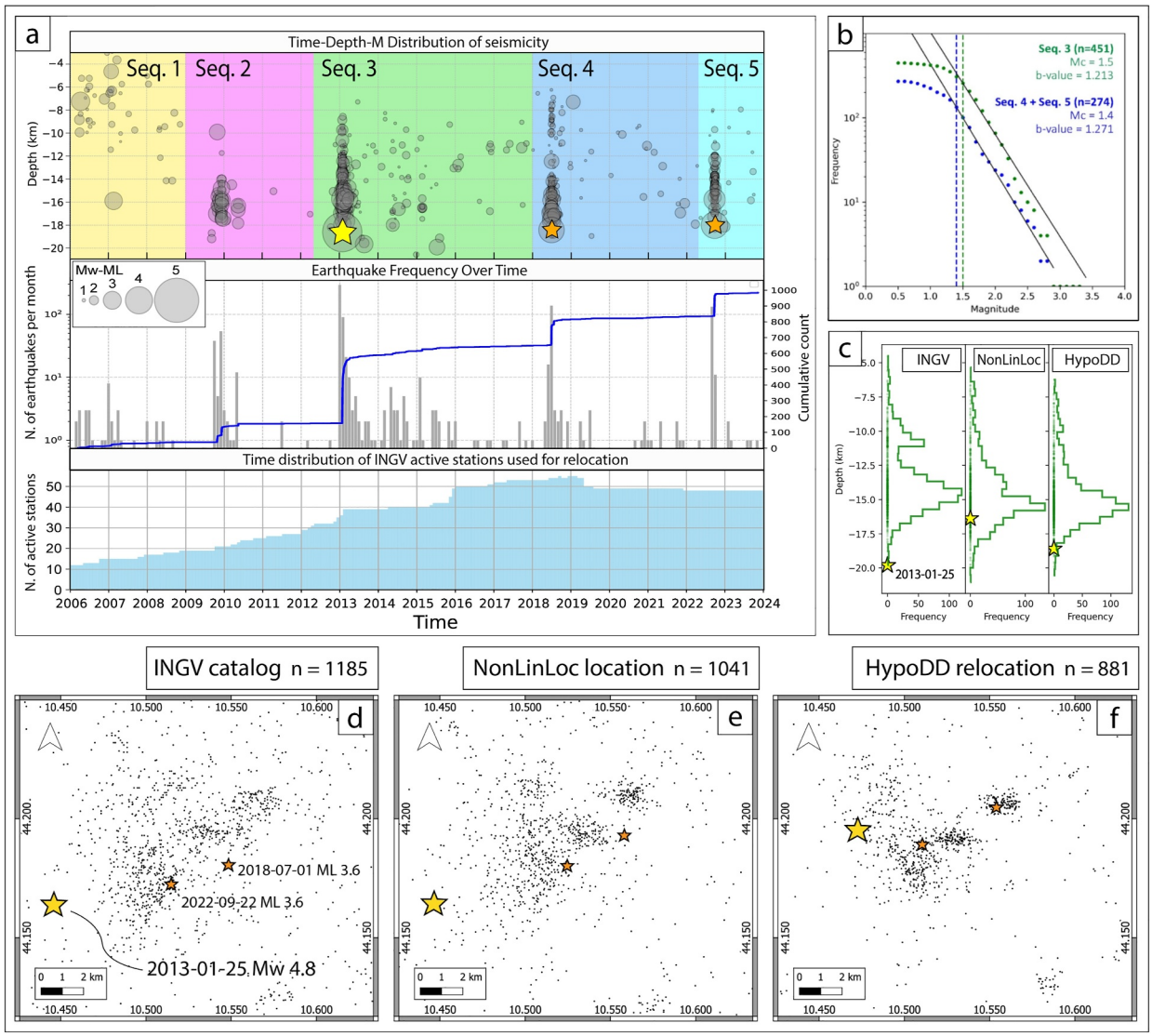


**Figure 4.** (a) 2006–2024 earthquakes time series, monthly earthquake rate and cumulative active stations though time. Panel (b) mc and b-value are calculated from original National Institute of Geophysics and Volcanology (INGV) catalog. (c) INGV, NLL, HypoDD catalogs events-depth histograms, with respective depth of the 2013 mainshock. (d)–(f) maps of earthquakes distribution within INGV, NLL and HypoDD catalogs, with stars indicating 2013 (yellow) and 2018–2022 (orange) largest earthquakes.

events pairs and individual residuals between theoretical and observed travel-times, under the assumption that nearby sources have almost identical ray paths and travel-times if the receiver is sufficiently distant. Given the large number of events, we used the LSQR conjugate gradient method (Paige & Saunders, 1982) to solve the system of DD equations. We tested a range of input parameters to minimize the number of events lost and the shift of earthquake cluster positions with respect to both INGV and NLL relocations, resulting in 881 relocated earthquakes (Figure 4d). Full parametrization is in Supporting Information S1. For each cluster, we graphically interpreted a single fault plane that best fits the distribution and density of earthquakes in 3D space. Each fault plane is a rectangle defined using Okada geographic, geometric and kinematic parameters (Figure 5b, Table S6 in Supporting Information S1).

### 3.2.3. Focal Mechanisms Computation

From all the available unfiltered vertical-component seismograms of the $M > 2.5$ earthquakes, we manually picked P polarities. We used HypoDD event-station azimuths and take-off angles to constrain 17 focal

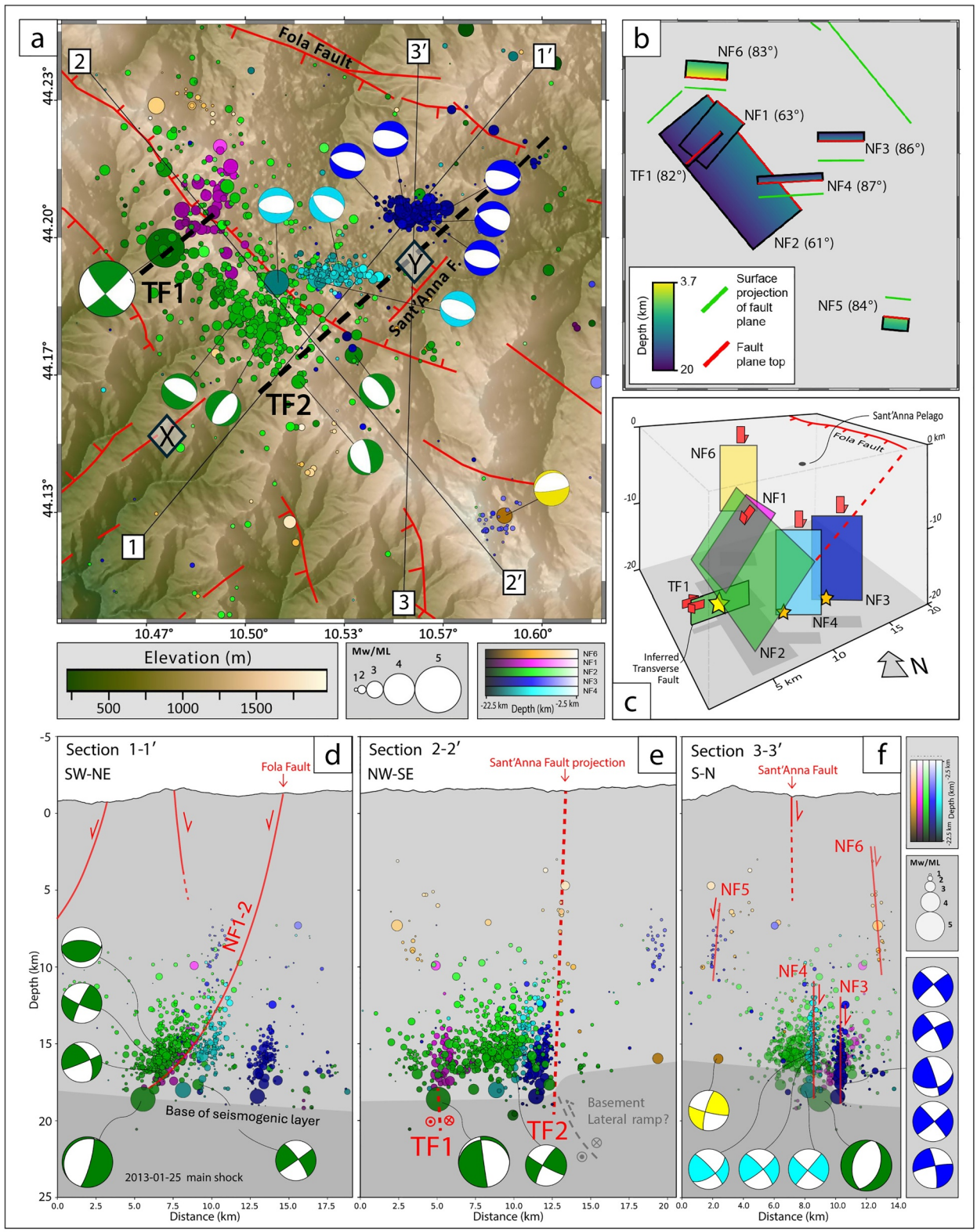


**Figure 5.** (a) Map showing double difference relocated epicenters (colored and seized by time, depth and magnitude), focal mechanisms (lower hemisphere), cross-sections traces in black and the locations of the historical $M > 4$ earthquakes (X, Y) and the inferred transverse fault traces TF1-2 in dashed black. (b) Map view and (c) schematic 3D sketch showing the main identified faults planes. (d)–(f) Cross-sections featuring faults (in red), projected hypocenters and focal mechanisms in lateral view (opposite hemisphere).

mechanisms using the grid-search approach in FOCMEC (Snoke, 2003). FOCMEC performs an efficient, systematic search of the focal sphere and reports acceptable solutions based on selection criteria for the number of polarity errors or using relatively-weighted factors (RW), in the way that a mismatch for data near a nodal surface counts less than a mismatch near the middle of the quadrant. Thanks to good azimuthal stations coverage, we were able to constrain focal mechanisms without exceeding 1 polarity errors or adopting RW > 0.2.

#### 3.2.4. Isola Santa-Sillico Fault System, Kinematic Data Analysis

To constrain the directions of shortening and extension associated with the development and re-activation of ISSF, we conducted a first order characterization of brittle structures by collecting geometric-kinematic data in its exhumed internal domains on the western flank of Garfagnana basin. Analysis has also been extended to Apenninic systems. The measured structures belong to: (a) main faults with displacement surfaces associated with cataclastic zones and indications of movement, (b) minor faults with indications of movement, (c) conjugate shear fracture systems. Sense indicators were inferred from steps on planes, R-T-fractures, ridge-in-groove striae and calcite growth fibers. General paleo-stress conditions were obtained with TENSOR (Delvaux & Sperner, 2003), following guidelines employed in close areas by Cortopassi et al. (2006), Ottria and Molli (2000), and Vaselli et al. (2008).

### 3.3. Location Results

#### 3.3.1. Relocation Performance and Catalog Comparison

To assess the quality of earthquake location and compare across the INGV, NLL and HypoDD catalogs we used the method proposed in Michele et al. (2019). We extracted the normalized values of the most common uncertainty estimators and combined them in a single inverse quality index spanning 0–1 using Michele et al. (2019) empirical relation. The values are associated with A to D quality classes. Estimators have been normalized to respective common maximum index values from all catalogs, within a 95% percentile. Normalization is needed to legitimize the combination of different physical quantities and comparison across catalogs.

Since the LQRS method from DD location doesn't provide reliable uncertainty estimations, overall location performance was tested using the SVD method on a reduced subset (∼100 earthquakes from the 2018 cluster), assuming that the resulting errors are representative of the entire data set.

Quality indices are graphically presented in the Figure S4 in Supporting Information S1 as histograms and quality class related median absolute deviations. Individual event error values for each catalog are provided in their respective Data Set S1–S4. Progressive improvement in event location is mainly indicated by decreasing median RMS values, from 0.200 s (std = 0.232) to 0.113 s (std = 0.067) and 0.068 s (std = 0.018) across the INGV, NLL, and HypoDD catalogs, respectively. Histograms of quality indices show a slight average improvement in the quality of NLL compared to INGV. The DD relocation achieve the lowest horizontal and vertical median errors.

Figure 4 compares the distribution of the three catalogs events, together with respective locations of the largest earthquakes from 2013, 2018 and 2022 clusters. The overall statistical improvement is consistent with the notable progressive improvement in swarm clustering shown in the NLL and HypoDD catalogs (Figure 4d). Depth distribution of the seismicity from the catalogs is in histogram form in Figure 4c. NLL and HypoDD events tend to occur at slightly greater depths on average compared to INGV events. Also, the 11 km depth artificial peak artifact within INGV catalog due to their over-simplified 1D velocity model (Latorre et al., 2023; Scudero et al., 2021) is not present in the NLL and HypoDD catalogs.

Of the DD relocated earthquakes 99.8%occur between 7 and 19 km depth, with 78% locating between 12 and 17 km depth. The average shifts of DD locations, in longitude, latitude and depth directions, compared to the NLL catalog are 0.6, 0.9, and 1.2 km, respectively. The largest horizontal shifts are observed for the deepest earthquakes. The 2013 mainshock indeed locates much closer to the aftershock cluster compared to both INGV and NLL catalogs.

To assess how NLL and HypoDD relocation shifts impacted the 2013 mainshock focal mechanism solutions and to compare them with the original INGV solution, we calculated them using NLL and HypoDD derived take-off angles and azimuth values. The results (Figure S3 in Supporting Information S1), consistently indicate near pure strike-slip kinematics for all solutions, with similarly oriented steep nodal planes. The solution obtained using the

HypoDD parameters was unambiguous and confirmed the strike-slip nature of the mainshock, with E-W oriented P-axes.

Given the DD improvement of location, we adopted the HypoDD catalog for analysis. Henceforth, following references will be exclusively made to HypoDD data.

### 3.3.2. Cluster Geometries, Kinematics and 3D Distribution of Seismicity

The DD solutions reveal the 3D spatial clustering of six sequences. For these sequences, we report the depth-magnitude-time evolution (Figure 4a). The most significant sequences occur in 2013, 2018, and 2022. Their largest earthquakes occurred at the very early stages, followed by a rapid Omori-like decay in aftershocks. Notably, each sequence starts with the largest earthquake located near the base of the respective cluster. Intervals of 2–4 years occurred between subsequent sequences.

We computed 15 focal mechanisms for events in the 2013, 2018 and 2022 sequences. Another solution was obtained for a singular 2007 ML = 2.8 deep event located in the SE part of study area. All focal mechanisms solutions are reported in Table S1 in Supporting Information S1. Figures 5a and 5d show sequences differentiated by time, depth, magnitude, together with the focal mechanism of the respective event. Fault geometries are summarized in sketch of Figure 5c and parameterized in Table S6 in Supporting Information S1. Dipping angles are in Figure 5b. The major aligned structures are:

- NF1: 2009–2010 cluster occurs as two distinct minor sub-sequences on 2009 and 2010 having no evidence of mainshock-aftershock relations. The largest event is ML = 2.8, and no focal mechanisms were computed. Hypocenters are ∼14–18 km-deep, and define a 3-km-long, SW dipping fault striking NW-SE.
- TF1: The 2013 $Mw = 4.8$ mainshock occurred on 25-01-2013 at 14:48 (UTC), at a depth of 18.6 km. Its focal mechanism indicates a strike-slip kinematic with Apenninic or transverse nodal planes. Given that Apenninic faults are characterized by dip-slip and only exhibit minor left-lateral components (Molli et al., 2021), we attribute this event to a transverse, near-vertical plane with right-lateral slip.
- NF2: 2013 aftershock cluster defines a ∼7-km-long, ∼10–18-km-deep SE striking fault, dipping to the SW. The first aftershock event occurred immediately after the mainshock, at 14:52 (UTC), followed by dense localized sequence. The 2013 seismicity is concentrated along a slightly curved structure with strike ranging from 325° in the southeast to 300° in the northwest, with the latter closely matching the strike and dipping angle of NF1. NF2 has been approximated as a planar surface with a 310° strike. The cluster is denser on the SE termination of the fault, and its centroid is planimetrically shifted on it about 2.5 km to the SE with respect to the mainshock, where all greater magnitude earthquakes occurred. Aftershocks on the fault plane decay rapidly, while sparse seismicity occurred till the end of 2017. All related focal mechanisms exhibit nearly pure normal kinematics, mainly on Apenninic striking nodal planes.
- NF3-NF4: 2018 (NF3) and 2022 (NF4) hypocenters define two dense, ∼3-km-long, ∼11–18-km-deep, E-W striking clusters fit by faults dipping steeply to the north and located at the footwall of NF2. Their respective largest 2018-07-01, ML = 3.6 and 2022-09-22, 3.7 earthquakes occurred at 18.4 and 18.0 km depth. All focal mechanisms indicate nearly pure normal slip on these faults, with only minor lateral components. All nodal planes have dip-angles spanning 40–80° and show strikes consistent with clusters' directions.
- NF5: on the SE sector a minor cluster is made by different 2018 earthquakes and aligns on a E-W striking high angle minor fault dipping to the S.
- NF6: Limited network coverage prevented relocation of some 2006–2007 events with NLL and HypoDD, so we used the original INGV locations, which already show good clustering on a minor E-W ∼5–10 km-depth, N-dipping HAFs.

Best-fitting fault planes are showed in map view in Figure 5b. The vertical cross-sections 1-1′, 2-2′, 3-3′ of Figure 5d, are perpendicular to NF2, NF3-4, and frontal to NF2, respectively. The main 2010, 2013, 2018, 2022 clusters exhibit a similar range in hypocenter depths. Their deepest events and the sparse seismicity describe a surface dipping at low angle (∼5°) to the NE, located at approximately 18 km in the SW and 20 km to the NE of the study region (Figure 4d). All 2013-2018-2019 largest earthquakes clearly lie on the 3D envelope of this limit. The seismicity in the area abruptly decreases toward the SE, just beyond the eastern tips of the 3 main clusters (Figure 4d).

10.1029/2025TC008859

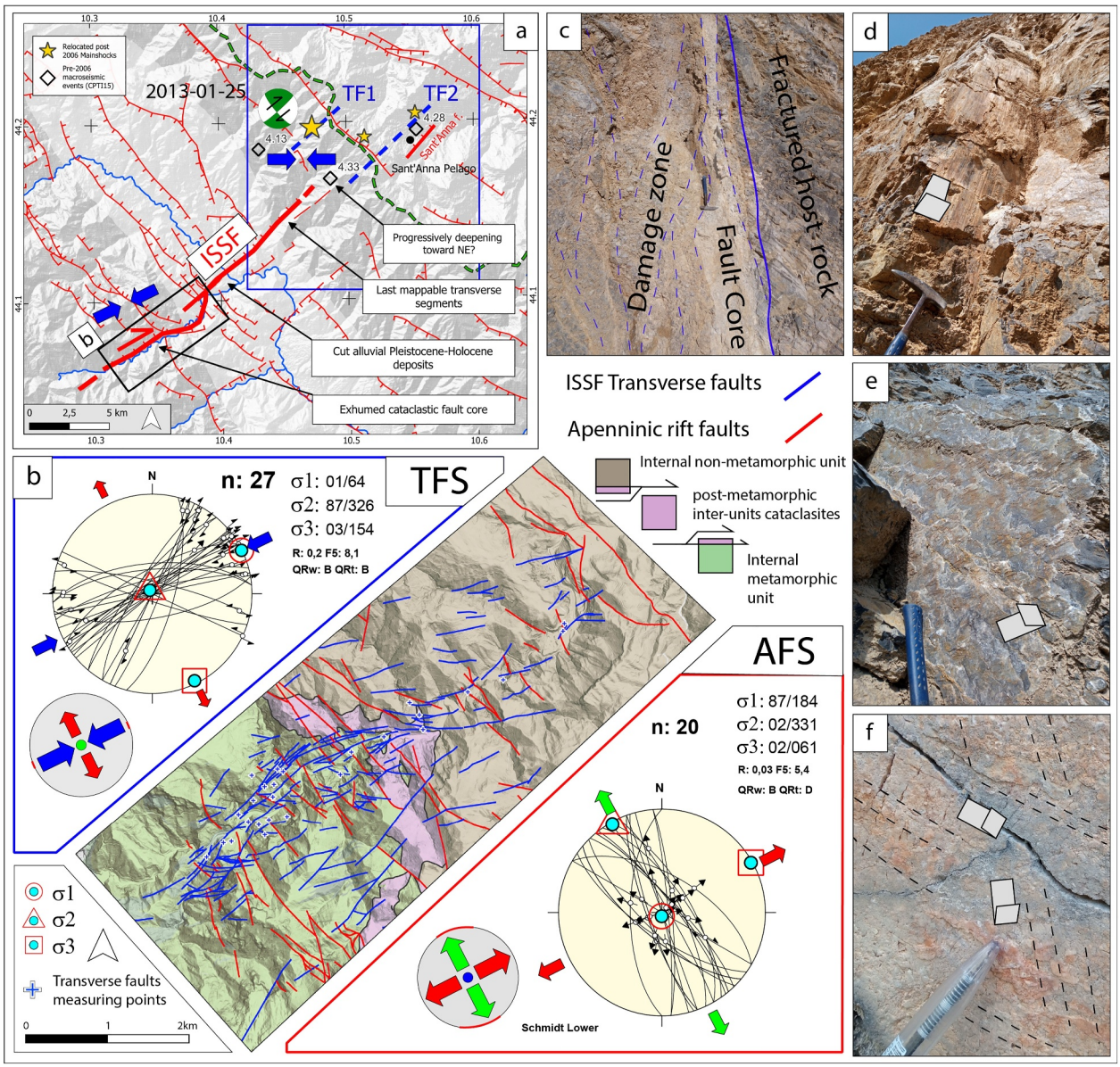


**Figure 6.** (a) Schematic map showing the Sant'Anna Pelago area, with the traces of TF1 and TF2, in dashed blue lines and Isola Santa-Sillico fault system (ISSF) (in red). Blue arrows indicate the paleo-to actual stress P-axes directions in internal and external sectors of ISSF. The black rectangle refers to the area in (b) Detailed map showing the high-angle fault architecture in the mapped area. Results of kinematic analyses are shown separately for the transverse (TFS) and the Apenninic fault systems. Sampling locations are shown with blue crosses. (c) Major Steep transverse fault zone with cataclastic fault core and anastomosing splays. (d) Minor dip-slip fault with kinematic indicators. (e) Transverse oblique-slip fault with slicken fibers. (f) Hybrid fault plane with two systems of sense indicators overlapping at high angle.

### 3.3.3. Isola Santa-Sillico Fault System: Geometric-Kinematics and Paleo-Stress Constrains

The ISSF is a major long-lived, 20-km-long transverse fault system nearly reaching the orographic divide (Figures 2, 3, and 6). Near its NE end, the system is active with linear sparse seismicity (INGV catalog), cross-cutting relations with recent Quaternary deposits (Di Naccio et al., 2013; Puccinelli, 1987; Puccinelli et al., 2016a, 2016b), hydrothermal upwelling and sinkholes (La Rosa et al., 2018; Molli et al., 2021). Along the western flank of the Garfagnana basin, the system is exhumed and dislocated by the east-dipping normal fault systems bounding the basin margin, through kilometer-scale throw. The system mainly develops within carbonate rocks, allowing for continuous tracing of multiple structures and geometries. Several sets of internal Apenninic normal faults also intersect the transverse system (Figure 6b). However, there are no univocal overlapping relationships between

transverse and Apenninic faults, with them likely being coeval. The transverse system is characterized by a series of highly segmented, steep to vertical corridors of localized deformation. In the innermost portion, the system transitions continuously from SW-NE to nearly E-W directions. Further north, the system becomes more segmented and discontinuous with NNE trending portions. Locally, in the field, two populations of oblique-dip-slip and strike-slip striae or fibers are associated with the same fault, showing oblique to ∼90° relations (Figure 6f). The kinematic data indicate that both the main SW-NE and E-W corridor sets are predominantly characterized by nearly pure right-lateral slip and minor dip-slip motion. In the main deformation zone the downthrown block is always that to the north for both systems. No unique overlap relations between dip-slip and lateral-slip striae on the same individual planes have been observed, further supporting potentially coeval dip- and strike-slip movements during intermittent mixed reactivation episodes. In addition to the main corridors, numerous sets of minor conjugate oblique left-lateral faults with ENE to ESE directions are present, which were essential for the inversion of the paleostress. The existence of pairs of sub-vertical conjugate fault systems suggests nucleation and initial stages of deformation occurred under vertical σ2 conditions.

For the inversion of the stress conditions of strike-slip systems, kinematics related to oblique strike-slip activations were analyzed alone. To constrain regional extension conditions, we inverted the tensors related only to movements recorded on the Apenninic dip-slip systems. The resulting paleostress tensors, shown in Figure 6b, indicate sub-horizontal ∼N64 oriented σ1 for strike-slip systems, and sub-horizontal ∼N61 oriented σ3 for dip-slip systems.

## 4. Coulomb Stress Change Calculation

Earthquakes can modify the stress state on nearby faults by either promoting or inhibiting slip (Harris, 1998; King et al., 1994; Lin & Stein, 2004; Stein, 1999; Toda et al., 2005). While positive stress changes caused by a fault slip (the source fault) on a pre-stressed fault (the receiver fault) can bring it to fail, negative stress changes unload faults, inhibiting their rupture. The CSC on a specified fault is independent of regional stress but depends on the fault geometry, sense of slip, and the coefficient of friction.

The aim of our analysis is to test whether the 2013, 2018, and 2022 sequences were stress-triggered by the 2013 $Mw = 4.8$ mainshock on the hypothesized TF1 deep transverse dextral strike-slip fault. This assessment was carried out by comparing the aftershocks distribution with the 3D stress-change pattern associated with the fault.

To relate the moment magnitude ($Mw$) of an earthquake to the average displacement ($d$) and the area of the slip surface ($S$), the empirical relation proposed by Hanks and Kanamori (1979) has been used:

$$M_w = \frac{2}{3}\log_{10}(Mo) - 6.03$$

where $Mo$ is the seismic moment in Newton*meters. The seismic moment is given by:

$$M_0 = \mu S d$$

where $\mu$ is the shear strength of the rock (assumed typical value $\mu = 3 \times 10^{10}$ N/m$^2$), $S$ is the area of the slip surface, $d$ is the average slip. $S$ value has been estimated from scaling relationship between fault rupture length and earthquake magnitude, at variable stress drop values (Hanks, 1977; Scholz, 2002). For a stress drop value of 10 MPa, consistent with the large depth of the system, and a $Mw = 4.8$ earthquake, a rupture fault length of approximately 2 km and a height of 1 km is expected. The average slip value we calculate is 0.3 m.

The spatial and geometrical properties of the fitted planes and fault kinematics parameters (Figure 7) were used to build the model for the static CSCs simulation using Coulomb 3.4 (Okada, 1992; Toda et al., 2011). Calculations are made in an elastic half-space with uniform isotropic elastic properties (Okada, 1992). The friction coefficient value for normal faults is gave by the relation $fs = -1/\tan(2\beta)$ from (Sibson, 1974), where β is the fault dip, which yields $fs = \sim 0.60$, a value consistent with the expected deep lithologies (Figure 1c).

For the 2013 mainshock source fault (TF1), we adopted the parameters of the transverse nodal plane. The fault trace was positioned so that the mainshock locates on its SW tip, assuming rupture happening on the tip. For NF2, NF3 and NF4 receiver faults, considering the mean kinematic attitude described by relative focal mechanism, we

10.1029/2025TC008859

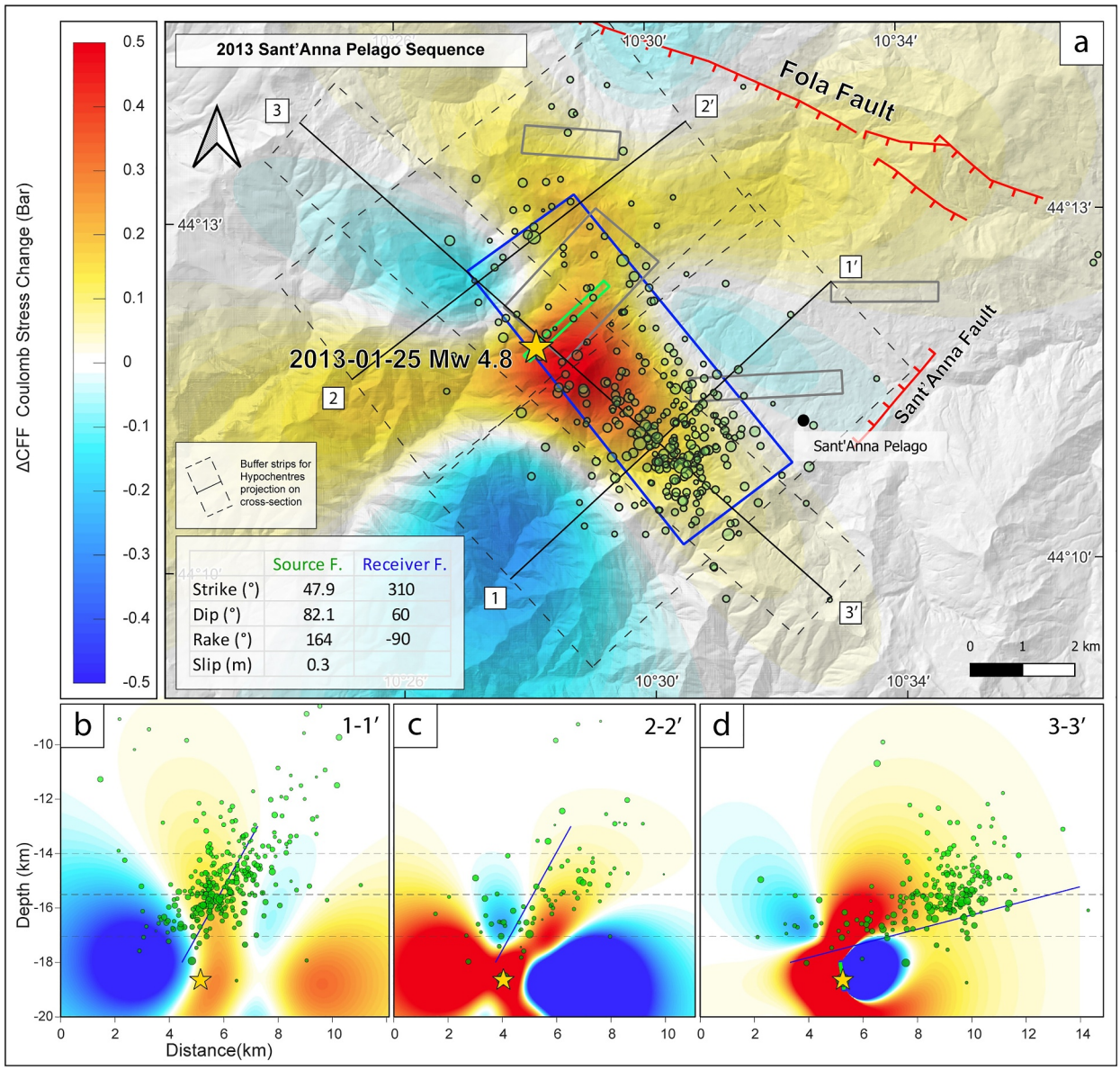


**Figure 7.** Static Coulomb Stress changes produced by the slip of the source fault TF1 on faults oriented like NF2 receiver fault, shown in horizontal section (a), built at 15.5 km of depth, and vertical cross-sections (b)–(d). The gray dashed lines indicate the projection steps used to filter the projection of the 2013 aftershock hypocenters (green dots) across sections.

use a normal dip-slip rake (−90°). Since only the 2013 mainshock exceeds $Mw = 4$, and the 2007 and 2010 sequences show no clear mainshock–aftershock relations, we assumed that NF1, NF2 and NF6 neither experienced appreciable slip nor caused significant stress changes. We therefore only use TF1 as the source fault. Figure 7 shows the resulting CSCs induced by TF1 activity on the 2013 receiver NF2, on several horizontal and vertical cross-section. Aftershocks are projected perpendicular to all sections, in order to optimally represent events within respective CSC fields. The results show a good correlation between distribution of positive CSCs and 3D aftershock distribution on NF2, with ∼85% of them being in the positive CSC lobes.

As shown in all the sections, the majority of aftershocks locate in the SE positive lobes, possibly as a consequence of the NW portion of the fault having already been unloaded during the 2010 sequence. CSC values across NF2 are low, spanning from 0.0025 MPa far from the mainshock to >0.05 MPa near the mainshock, at seismogenic depths. These results are close to hypothesized CSCs triggering threshold of 0.01–0.05 MPa in literature (King et al., 1994; Stein, 1999). Larger positive CSC plumes occurred at significant depths, beyond cutoff depths, where

co-seismic deformation likely doesn't occur. Other positive lobes are observed at the footwall of the Fola Fault, but no seismic activity has been recorded, suggesting a lack of Apenninic HAFs to activate and/or insufficient CSC to trigger seismicity. CSC tests on NF3 and NF4 showed that TF1 movement induced only minor negative stress changes (0.002–0.01 MPa), making triggering unlikely and suggesting that 2013 and 2018–2022 sequences were independent, as also suggested by the relatively long-time span between these events.

## 5. Discussion

### 5.1. Active Structures and Seismotectonic Implications

The precise relocation of seismicity indicates slip along five independent normal faults active during the last 17 years (Figure 5). The ∼NNE average T-axis orientation derived from the focal mechanisms of these faults is consistent with the regional minimum horizontal stress (Shmin) direction of the Apennines extensional systems (Figures 1c and 5). The consecutive 2010 and 2013 sequences are connected to the slip of adjacent portions of the same SW-dipping major fault system. Based on the position and shape of the two clusters and focal mechanism nodal planes we interpret them as being on the Fola fault (Figure 5), a regionally extended normal fault system with a significant morphological indication, and with kilometer-scale throw (Balocchi, 2020; Martelli et al., 2016a, 2016b). The seismicity on the fault extends down to the base of the seismogenic layer at ∼18 km. The other active faults modeled from seismicity have no direct surficial expression. Seismological observations also allow us to infer the presence of a sub-vertical major transverse fault TF2 (Figures 5a and 5d). This fault: (a) envelopes the eastern tips of the main 2013, 2018 and 2022 clusters, (b) aligns with the abrupt decrease of the seismicity to the SE, (c) aligns with the shallowing (∼1.5 km) of the seismogenic layer toward the SE, (d) runs parallel to the near-surfacing transverse Sant'Anna fault, (e) broadly coincides with the location of the 1988 $Mw = 4.28$ and 1997 $Mw = 4.33$ (Rovida et al., 2022) historical earthquakes (X, Y in Figure 5a), located at depths of 18, 6 and 16 km, respectively. The Sant'Anna fault could represent the local surface expression of TF2. TF2 likely cross-cuts the Fola fault at depth and acted as a major barrier during the 2013 aftershock sequence, inhibiting propagation of rupture toward the east (Pace et al., 2002; Pizzi et al., 2017).

Relocation has shown 4 sub-vertical W-E striking faults, including en echelon NF3 and NF4 at the footwall of the Fola fault. The E-W trend is common in this region and many major fault systems exhibit curved trajectories with E-W strike at the eastern terminations. HAFs exhibit these trends where they overprint former curved or E-W oriented tectonic elements related to the compressional phase, such as concave oblique ramps between main frontal ramps (Figure 3). However, as the inferred faults are oriented parallel to the 2013 mainshock P axis and are subvertical, we believe they may have nucleated as en echelon tension or strike-slip structures under the same stress field, and recently reactivated as normal faults in a transtensional regime. As the eastern tips of NF3 and NF4 coincide with TF2, they might be originated as synthetic splays related to it. As none of the computed solutions show true vertical nodal planes which align with the overall geometry of the clusters, slip may have occurred on multiple minor medium-angle en echelon splays above an overall steep structure. Our CSC analysis additionally support the presence of the separate deep, dextral transverse fault TF1 (Figure 7), located 7 km NW of TF2 at the base of the seismogenic crust, and consistent with the northeast-oriented nodal plane of the 2013 mainshock focal mechanism. The data support that mainshock and aftershock sequences occurred separately on distinct, orthogonally oriented faults, reinforcing the inconsistency of left-lateral slip at depth transitioning to dip-slip at shallower levels along the same fault plane. As the 2013 mainshock broadly locates between NF1 and NF2 we hypothesize that TF1 may act as a deep seismic barrier, partially preventing the 2010 and 2013 sequences to overlap laterally (Figure 5d). Our findings support that the 2013 mainshock triggered the shallower Apenninic Fola fault. Given that the calculated CSCs are minimal and approach the typical failure threshold, it is likely that the fault was already near failure, likely due to the inter-seismic loading.

ISSF tips just a few kilometers southwest of the Sant'Anna area (Molli et al., 2021; Martelli et al., 2016a, 2016b). As this system approaches the orographic divide, evidence of transverse structures disappears (Figures 2 and 6a). NE of the divide, only the small-scale Sant'Anna fault exists. The geometric-kinematic analysis on the exhumed part of ISSF aimed to identify analogies with the inferred geometries and active deep kinematics in the Sant'Anna area. The high angle multi-splay nature of ISSF is consistent with our findings in the external sectors, where TF1 and TF2 are steep and parallel. Paleostress reconstruction on the transverse strike-slip faults reveals a stress field consistent with that of the 2013 mainshock (Figure 6b). In addition, inversion of coeval Apenninic normal faults data near the ISSF shows a NE-directed σ3, fully in agreement with the orientations of the GNSS velocity vectors

(Bennett et al., 2012; Molli et al., 2021; Serpelloni et al., 2022), and the current stress regime (Mariucci & Montone, 2024; Montone & Mariucci, 2016) near the Sant'Anna region (Figure 1c).

The internal ISSF shares several geometric and kinematic features with the nearby major transverse North Apuan Fault (NAF) System (NAF, Figure 2) to the W, including an anastomosing, multi-corridor architecture with variably oriented faults, an overall transtensional behavior, indicated by oblique-normal kinematics on the transverse planes (Molli et al., 2015) and signs of ascending hydrothermal fluids (La Rosa et al., 2018; Molli et al., 2015). In the Sant'Anna area, the combined σ3 orientations from all observed active faults (NE for NF2-3 and N for NF3-4-5 and TF1) result in NNE-oriented extension, consistent with both the extension direction inferred from field data on the NAF (Molli et al., 2015) and its current Shmin orientation (Figure 1c).

### 5.2. Regional Tectonic Significance

Recent studies suggest that active extensional deformation in the high elevated tip of Northern Apennines is completely accommodated within a complex HAF architecture (Molli et al., 2021; Saccorotti et al., 2022). Our observed fault geometries, kinematics, and seismicity distribution also point to this structural configuration, which contrasts with earlier interpretations involving low-angle detachments (Boncio et al., 2000; Di Naccio et al., 2013; Eva et al., 2014; Meletti et al., 2008; Pezzo et al., 2014; Stramondo et al., 2014). However, the physical nature of the ∼18 km deep boundary below which seismic activity ceases remains uncertain due to limited deep geophysical data in the region. This boundary may represent either the basement top of an external unit, as suggested by Molli (2008), or possibly the brittle-ductile transition zone.

While we document the existence of transverse faults and their interaction with rift-related structures the reasons for the existence, and origin of these transverse faults in the study area are not completely clear. Interpretations of transverse faults across the Apennine chain are often contrasting, particularly when looking at different tectonic domains. Numerous contributions have recognized crustal shortening and/or pre-orogenic structural inheritance as key preconditions for the formation of late transverse HAFs, identified in various settings and different structural levels within the Apennine orogen (Acocella & Funiciello, 2006; D'Agostino et al., 1998; Faccenna et al., 1995; Liotta, 1991; Milia & Torrente, 2015; Pascucci et al., 2007; Pizzi & Galadini, 2009; Tavarnelli et al., 2001; Vannoli et al., 2015, 2016). Transverse faults in rifted thrust-and-fold belts are believed to arise from the inherited lateral segmentation of the continental margin that existed before subduction, and/or structural features acquired during subduction process itself (Calassou et al., 1993; Homberg et al., 2002; Jiménez-Bonilla et al., 2020; Tavani et al., 2020, 2021). Transverse faults are seen to directly propagate to the sedimentary covers from pre-existing structures in the continental basement, controlling segmentation of thrust systems within the outer active contractional belt (Costa et al., 2021, 2023; Mazzoli et al., 2014; Vannoli et al., 2015) and rift systems (Pizzi & Galadini, 2009). Inheritance of former structures has also been documented in central Tuscany, where major late transverse faults are interpreted as reactivated discontinuities within the upper wedge levels, originally transferred from oceanic material to the orogen during subduction (Nirta et al., 2007; Rosenbaum & Piana Agostinetti, 2015).

Alternative mechanisms such as rotational tectonics or complex dynamics within the wedge/slab system has often considered to be a sufficient forcing mechanism to newly form structural lineaments oriented perpendicular to the tectonic fronts, as products of local differential movements within prograding thrust-and-fold belt (Rosenbaum et al., 2008), or changes in foreland monocline dipping angle have been proposed (Mariotti & Doglioni, 2000). Examples exist from both exhumed (Benini & Farabegoli, 1990) and buried foreland external domains (Bigi et al., 1990; Costa et al., 2023; Diss Working Group, 2021; Mazzoli et al., 2014; Vannoli et al., 2015; Vannucchi et al., 2012) (Figure 1a). Other examples are from the northern rift tip, where transverse HAFs has shown to reflect significant longitudinal heterogeneities within the basement, acquired during a multi-stage structural evolution involving concurrent lateral accommodation of thrust sheets and differential crustal thinning by early low-angle normal faults (Molli et al., 2018). Both wedge and rift segmentation appear here to localize along a few main corridors, corresponding to major transverse structures such as the NAF, the Sillaro (Bettelli & Panini, 1992; Vannucchi et al., 2012), and Taro fault systems (Bernini & Papani, 2002; Eva et al., 2014) (Figure 1a). Another significant contribution in interpreting late transverse faults comes from several authors studying the rift domains south of the Livorno–Empoli Line (Figure 1a). In these regions, where the crust is overthinned and finite deformation is dominated by extensional features, some transverse faults are interpreted as not related to pre-existing structures (Brogi et al., 2023, 2024; Liotta and Brogi, 2020; Liotta et al., 2015; Mirabella

et al., 2022). These studies suggest the presence of newly formed, medium-to high-angle, distributed and anastomosing Miocene–Pliocene transtensional transverse faults that accommodate differential extension (Gola et al., 2017; Liotta & Brogi, 2020). Such transverse faults are thought to have control on time-space distribution of crustal permeability (Acocella & Funiciello, 2006; Brogi et al., 2010, 2014; Rosenbaum et al., 2008) as deformation progressively propagates eastward over time.

Whether the tranverse faults in our study area are inherited, newly formed or related to the propagation of the ISSF tip in concert with the eastward migration of the extensional front is unclear. However, several observations support the inherited hypothesis. The finite deformation state of the tectonic elements near the orographic divide, associated with both shortening and extension and morphological features in the region, is primarily marked by gradual eastward left-stepping offsets within an overall en echelon pattern. In the Sant'Anna area, the along-strike segmentation of the wedge is characterized by significant leftward steps affecting both the internal and external unit fronts. A major step is observed as an ∼8 km eastward advance of the internal unit front. The curved trends of the frontal to oblique ramp folds, within both the internal and external units, are overprinted by prominent eastward-curving, NE-dipping HAFs. This step may correspond to either a thrust-sheet frontal fold lateral tip or a highly oblique to orthogonal ramp structure accommodating sinistral shear (Figure 3). No field evidence of wedge offset indicative of lateral ramps has been documented. However, the step aligns with the northeastern projection of the ISSF (Figures 3a and 6a), suggesting a possible link between the segmentation of the orogenic wedge and that of the late rift fault system. This relationship may be explained by the superimposition of rift-related transverse faults onto pre-existing inherited structures. In addition, the low amounts of extension, young age, and lack of spatial changes in extension rate make it difficult to explain the presence of the transverse faults without inheritance (Acocella & Funiciello, 2006).

We propose that extension initiates as left-stepping basins that are kinematically linked by dextral transverse fault systems, superimposing on left-stepping thrust wedge. In this scenario, deformation within the lateral steps between extensional zones may be accommodated at depth by the reactivation of pre-existing, orthogonally oriented regional structures. We suggest that the Sant'Anna Pelago area represents a high topography immature zone of extension where the main visible tectonic signature in the field is still that of contraction. Transtension may arise along the NE continuation at depth of the transverse ISSF, and may superimpose on former transverse inherited elements, but structural connections between deep-seated structures and topography are not fully established here. In contrast, more extended internal domains show clear morphological expression of extension and faults have high angle relationships, as extension had more time to superimpose on contractional features. The ISSF zone may correspond to a mature domain equivalent to that of Sant'Anna Pelago, where fault network had time to evolve to hard-linkage arrangement.

We suggest that the Northern Apennines is a key region to delve deeper into the problem of continental transverse structures and how they evolve with time. In particular, this region is interesting because it captures an active tectonic transition, where areas previously dominated by contractional stresses are now experiencing extension. These recently extended domains already exhibit semi-evolved transverse structures and provide a unique opportunity to observe and analyze these structures during their developmental stages.

### 5.3. Broader Implications

Young basins in the early stages of continental rifting typically exhibit complex faults networks and transfer zones that accommodate strain between offset fault segments (Corti, 2008; Green et al., 2014; La Rosa et al., 2022; Macdonald et al., 1988; Taylor et al., 2009; Tyler et al., 2007; Willemse et al., 1997). In traditional models these systems evolve through time so that major strike-slip faults oriented parallel or highly oblique to extension develop only in mature rifts approaching seafloor spreading (Storti et al., 2007), with oceanic transform faults being the classic example (Allken et al., 2012; Eagles et al., 2015; Nguyen et al., 2016; Taylor et al., 2009). Alternative studies show that proto-transform faults can evolve from long-lived continental linkage zones during the final stages of rifting, prior to continental breakup (Behn & Lin, 2000; Cochran & Martinez, 1988; Illsley-Kemp et al., 2018; McClay & Khalil, 1998).

The Apennines stand as a notable exception, since observable orthogonal strike-slip structures initiate during the earliest phases of extension, as in Sant'anna Pelago area. We interpret this early development to the inheritance of transfer faults that are pre-orogenic or originally formed associated with the thrust-and-fold system. The Apennines may represent a key area to investigate how pre-existing transverse faults evolve as they progress from

the undeformed foreland, through the orogenic belt, and into internal extensional domains at varying stages of extension (Jolivet et al., 1998; Kastens & Mascle, 1990; Savelli & Ligi, 2017; Tavani et al., 2021).

## 6. Conclusion

We conducted an integrated study of the Sant'Anna Pelago area, a key region to study seismicity along crustal structures oriented almost parallel to the compressional stresses responsible for the Northern Apennines orogeny. Our work included precise relocation of post-2006 seismic sequences, a critical review of existing geological maps, geological-structural analysis, and static CSC calculations. Based on our relocation, we document a systematic pattern of active faulting near the extensional front. The system features two deep-rooted transverse faults accompanied by shallower normal faults in two distinct orientations following both the NW-SE Apenninic trend and an E-W direction. These structures operate as an integrated tectonic system. The CSCs analysis supports that one of the transverse faults is the possible source candidate of the deep 2013 strike-slip mainshock. Its kinematics is consistent with that identified from paleostress analysis in the exhumed internal portions of the transtensive ISSF. This correspondence suggests that newly identified active transverse faults may be connected to the deep, northeast subsurface prosecution of the ISSF, mirroring the multisplay structure of exposed ISSF segments. TF2 appears as a well-developed, crustal-scale fault capable of inhibiting the propagation of rupture along the Fola Apenninic fault. In contrast, TF1 represents an early-stage structure confined at the base of the seismogenic layer, which has proven to directly bring the major Fola fault closer to failure. These structures align coherently with a major transverse structure that extend across the Apennines and orographic divide. We therefore interpret the transverse structure to be inherited from either the pre-contractional or contractional phase.

The Sant'Anna Pelago area represents an immature transtensional soft-linkage zone where new extensional structures are beginning to superimpose on the contractional wedge and to develop its surface fault architecture. These findings have significant implications for the regional seismotectonic setting of the study area and show that transverse faults can be seismogenic, can accommodate strike-slip motion and can be able to trigger slip along rift normal faults.

## Data Availability Statement

The earthquake data supporting this research are publicly available from the INGV catalogue (Istituto Nazionale di Geofisica e Vulcanologia, 2005). Used phase, station, and waveform are from the Italian National Seismic Network, operated by INGV and archived in the EIDA archive (Danecek et al., 2021). Absolute location calculations were conducted using the NonLinLoc (Lomax et al., 2000). Double-difference relocations were performed using the HypoDD (Waldhauser, 2001). Focal mechanisms were determined using the FOCMEC (Snoke et al., 1984). Coulomb stress changes were calculated using Coulomb 3.4 (Toda et al., 2011). Maps were created using PyGMT (Tian et al., 2024) and QGIS.

**Acknowledgments**
We sincerely thank the Editor, the Associate Editor, and the anonymous reviewers for their constructive comments, which significantly improved the manuscript. This work was funded by the SL PhD scholarship from the Department of Earth Sciences, University of Florence. DK was funded by NERC grant NE/L013932/1. Open access publishing facilitated by Universita degli Studi di Firenze, as part of the Wiley - CRUI-CARE agreement.

## References

Acocella, V., & Funiciello, R. (2006). Transverse systems along the extensional Tyrrhenian margin of central Italy and their influence on volcanism. *Tectonics*, *25*(2), TC2003. https://doi.org/10.1029/2005TC001845

Albarello, D., Batini, F., Bianciardi, P., Ciulli, B., Spinelli, E., & Viti, M. (2005). Stress field assessment from ill-defined fault plane solutions: An example from the Larderello geothermal field (western Tuscany, Italy). *Bollettino della Societa Geologica Italiana*, *3*, 187–193. [Google Scholar].

Allken, V., Huismans, R. S., & Thieulot, C. (2012). Factors controlling the mode of rift interaction in brittle-ductile coupled systems: A 3D numerical study. *Geochemistry, Geophysics, Geosystems*, *13*(5), Q05010. https://doi.org/10.1029/2012GC004077

Balocchi, P. (2020). Tectonics and seismotectonics of high dragone valley between piandelagotti and Montefiorino villages (northern Apennines, Italy). *Atti Società Toscana Scienze Naturali, Memorie, Serie A*, *127*, 29–39. https://doi.org/10.2424/ASTSN.M.2020.01

Basili, R., & Barba, S. (2007). Migration and shortening rates in the northern Apennines, Italy: Implications for seismic hazard. *Terra Nova*, *19*(6), 462–468. https://doi.org/10.1111/J.1365-3121.2007.00772.X

Behn, M. D., & Lin, J. (2000). Segmentation in gravity and magnetic anomalies along the US East Coast passive margin: Implications for incipient structure of the oceanic lithosphere. *Journal of Geophysical Research*, *105*(B11), 25769–25790. https://doi.org/10.1029/2000JB900292

Ben-Avraham, Z., & Ten Brink, U. (1989). Transverse faults and segmentation of basins within the dead sea rift. *Journal of African Earth Sciences*, *8*(2), 603–616. https://doi.org/10.1016/S0899-5362(89)80047-8

Benedetti, L., Tapponnier, P., King, G. C. P., Meyer, B., & Manighetti, I. (2000). Growth folding and active thrusting in the Montello region, Veneto, northern Italy. *Journal of Geophysical Research*, *105*(B1), 739–766. https://doi.org/10.1029/1999JB900222

Benini, A., & Farabegoli, E. (1990). Tettonica trasversale nell'Appennino forlivese. La Linea del Bidente. *Memorie Descrittive Carta Geologica d'Italia*, *46*, 245–255. [Google Scholar].

Bennett, R. A., Serpelloni, E., Hreinsdóttir, S., Brandon, M. T., Buble, G., Basic, T., et al. (2012). Syn-convergent extension observed using the RETREAT GPS network, northern Apennines, Italy. *Journal of Geophysical Research*, *117*(4), B04408. https://doi.org/10.1029/2011JB008744

Bernini, M., & Papani, G. (2002). Distensione della fossa tettonica della Lunigiana nordoccidentale (con carta geologica alla scala 1:50.000). *Bollettino della Societa Geologica Italiana*, *121*, 313–341. [Google Scholar].

Bettelli, G., & Panini, F. (1992). *Liguridi, melanges e tettoniti lungo la linea del Sillaro (Appennino settentrionale, Provincie di Firenze e Bologna)* (Vol. 46, pp. 387–415). Memorie Descrittive della Carta Geologica d'Italia. Retrieved from https://hdl.handle.net/11380/741418

Bigi, G., Castellarin, A., Coli, M., Dal Piaz, G. V., Sartori, R., Scandone, P., & Vai, G. B. (1990). Structural model of Italy scale 1:500.000, sheet 1. C.N.R., progetto finalizzato geodinamica, SELCA firenze. [Google Scholar].

Boccaletti, M., Corti, G., & Martelli, L. (2011). Recent and active tectonics of the external zone of the Northern Apennines (Italy). *International Journal of Earth Sciences*, *100*(6), 1331–1348. https://doi.org/10.1007/S00531-010-0545-y

Boccaletti, M., Elter, P., & Guazzone, G. (1971). Plate tectonic models for the development of the western alps and northern Apennines. *Nature; Physical Science*, *234*(49), 108–111. https://doi.org/10.1038/physci234108a0

Boncio, P., Brozzetti, F., & Lavecchia, G. (2000). Architecture and seismotectonics of a regional low-angle normal fault zone in central Italy. *Tectonics*, *19*(6), 1038–1055. https://doi.org/10.1029/2000TC900023

Bonini, M., Corti, G., Donne, D. D., Sani, F., Piccardi, L., Vannucci, G., et al. (2016). Seismic sources and stress transfer interaction among axial normal faults and external thrust fronts in the northern Apennines (Italy): A working hypothesis based on the 1916–1920 time–space cluster of earthquakes. *Tectonophysics*, *680*, 67–89. https://doi.org/10.1016/j.tecto.2016.04.045

Brogi, A., Capezzuoli, E., Martini, I., Picozzi, M., & Sandrelli, F. (2014). Late quaternary tectonics in the inner northern Apennines (siena basin, southern Tuscany, Italy) and their seismotectonic implication. *Journal of Geodynamics*, *76*, 25–45. https://doi.org/10.1016/j.jog.2014.03.001

Brogi, A., Liotta, D., Capezzuoli, E., Matera, P., Kele, S., Soligo, M., et al. (2020). Travertine deposits constraining transfer zone neotectonics in geothermal areas: An example from the inner Northern Apennines (Bagno Vignoni-Val d'Orcia area, Italy). *Geothermics*, *85*, 101763. https://doi.org/10.1016/J.GEOTHERMICS.2019.101763

Brogi, A., Liotta, D., Dini, A., & Rielli, A. (2023). Geology of montecastelli pisano (inner northern Apennines, Italy): Normal and transfer fault zones affecting a dismantled ophiolite bearing orogenic wedge. *Journal of Maps*, *19*(1), 2242723. https://doi.org/10.1080/17445647.2023.2242723

Brogi, A., Liotta, D., Meccheri, M., & Fabbrini, L. (2010). Transtensional shear zones controlling volcanic eruptions: The middle Pleistocene Mt amiata volcano (inner northern Apennines, Italy). *Terra Nova*, *22*(2), 137–146. https://doi.org/10.1111/j.1365-3121.2010.00927.x

Brogi, A., Vannoli, P., Zucchi, M., Burrato, P., Fracassi, U., Valensise, G., et al. (2024). Reappraising the seismogenic potential of a low-strain rate region: Active faulting in the eastern Siena Basin (southern Tuscany, Italy). *Tectonophysics*, *886*, 230423. https://doi.org/10.1016/j.tecto.2024.230423

Buonasorte, G., Fiordelisi, A., & Rossi, U. (1987). Tectonic structures and geometric setting of the vulsini volcanic complex. *Periodico di Mineralogia*, *56*, 123–136. [Google Scholar].

Burrato, P., Ciucci, F., & Valensise, G. (2003). An inventory of river anomalies in the Po Plain, Northern Italy: Evidence for active blind thrust faulting. *Annals of Geophysics*, *46*(5), 865–882. https://doi.org/10.4401/ag-3459

Calassou, S., Larroque, C., & Malavieille, J. (1993). Transfer zones of deformation in thrust wedges: An experimental study. *Tectonophysics*, *221*(3–4), 325–344. https://doi.org/10.1016/0040-1951(93)90165-G

Cantini, P., Testa, G., Zanchetta, G., & Cavallini, R. (2001). The Plio–Pleistocene evolution of extensional tectonics in northern Tuscany, as constrained by new gravimetric data from the Montecarlo Basin (lower Arno Valley, Italy). *Tectonophysics*, *330*(1), 25–43. https://doi.org/10.1016/S0040-1951(00)00217-1

Caricchi, C., Cifelli, F., Sagnotti, L., Sani, F., Speranza, F., & Mattei, M. (2014). Paleomagnetic evidence for a post-eocene 90° CCW rotation of internal apennine units: A linkage with corsica-sardinia rotation? *Tectonics*, *33*(4), 374–392. https://doi.org/10.1002/2013TC003364

Carmignani, L., & Kligfield, R. (1990). Crustal extension in the northern Apennines: The transition from compression to extension in the alpi apuane core complex. *Tectonics*, *9*(6), 1275–1303. https://doi.org/10.1029/TC009I006P01275

Cenni, N., Viti, M., Baldi, P., Mantovani, E., Bacchetti, M., & Vannucchi, A. (2013). Present vertical movements in Central and Northern Italy from GPS data: Possible role of natural and anthropogenic causes. *Journal of Geodynamics*, *71*, 74–85. https://doi.org/10.1016/j.jog.2013.07.004

Chiarabba, C., Jovane, L., & Di Stefano, R. (2005). A new view of Italian seismicity using 20 years of instrumental recordings. *Tectonophysics*, *395*(3), 251–268. https://doi.org/10.1016/j.tecto.2004.09.013

Chorowicz, J. (1989). Transfer and transform fault zones in continental rifts: Examples in the Afro-Arabian Rift System. Implications of crust breaking. *Journal of African Earth Sciences*, *8*(2–4), 203–214. https://doi.org/10.1016/S0899-5362(89)80025-9

Clemenzi, L., Molli, G., Storti, F., Muchez, P., Swennen, R., & Torelli, L. (2014). Extensional deformation structures within a convergent orogen: The Val di Lima low-angle normal fault system (Northern Apennines, Italy). *Journal of Structural Geology*, *66*, 205–222. https://doi.org/10.1016/j.jsg.2014.05.019

Cochran, J. R., & Martinez, F. (1988). Evidence from the northern Red Sea on the transition from continental to oceanic rifting. *Tectonophysics*, *153*(1–4), 25–53. https://doi.org/10.1016/0040-1951(88)90006-6

Coltorti, M., Farabollini, P., Gentili, B., & Pambianchi, G. (1996). Geomorphological evidence for anti-Apennine faults in the Umbro-Marchean Apennines and in the peri-Adriatic basin, Italy. *Geomorphology*, *15*(1), 33–45. https://doi.org/10.1016/0169-555X(95)00117-N

Conti, P., Cornamusini, G., & Carmignani, L. (2020). An outline of the geology of the northern Apennines (Italy), with geological map at 1: 250,000 scale. *Italian Journal of Geosciences*, *139*(2), 149–194. https://doi.org/10.3301/IJG.2019.25

Corti, G. (2008). Control of rift obliquity on the evolution and segmentation of the main Ethiopian rift. *Nature Geoscience*, *1*(4), 258–262. https://doi.org/10.1038/ngeo160

Corti, G., Maestrelli, D., & Sani, F. (2022). Large-to local-scale control of pre-existing structures on continental rifting: Examples from the Main Ethiopian Rift, East Africa. *Frontiers in Earth Science*, *10*, 808503. https://doi.org/10.3389/feart.2022.808503

Cortopassi, A., Molli, G., & Ottria, G. (2006). Studio della deformazione fragile nel bacino marmifero di Fantiscritti (Alpi Apuane, Carrara) finalizzato alla ricostruzione del campo di paleostress. *Geologia Tecnica and Ambientale*, *1–2*, 27–45. [Google Scholar].

Costa, M., Chicco, J., Invernizzi, C., Teloni, S., & Pierantoni, P. P. (2021). Plio–quaternary structural evolution of the outer sector of the marche Apennines south of the conero promontory, Italy. *Geosciences*, *11*(5), 184. https://doi.org/10.3390/geosciences11050184

Costa, M., Invernizzi, C., Penza, G., Teloni, S., & Pierantoni, P. P. (2023). Seismotectonic role of transversal structures in the Plio-Quaternary evolution of the external Marche Apennines (Italy). *Journal of the Geological Society*, *180*(6), jgs2023-002. https://doi.org/10.1144/jgs2023-002

D'Agostino, N., Chamot, R. N., Funiciello, R., Jolivet, L., & Speranza, F. (1998). The role of preexisting thrust faults and topography on the styles of extension in the Gran Sasso Range (central Italy). *Tectonophysics*, *292*(3–4), 229–254. https://doi.org/10.1016/S0040-1951(98)00070-5

Danecek, P., Pintore, S., Mazza, S., Mandiello, A., Fares, M., Carluccio, I., et al. (2021). The Italian node of the European integrated data archive [Dataset]. *Seismological Research Letters*, *92*(3), 1726–1737. https://doi.org/10.1785/0220200409

Dannowski, A., Kopp, H., Grevemeyer, I., Lange, D., Thorwart, M., Bialas, J., & Wollatz-Vogt, M. (2020). Seismic evidence for failed rifting in the ligurian basin, western alpine domain. *Solid Earth*, *11*(3), 873–887. https://doi.org/10.5194/se-11-873-2020

Dawson, S. M., Laó-Dávila, D. A., Atekwana, E. A., & Abdelsalam, M. G. (2018). The influence of the Precambrian Mughese Shear Zone structures on strain accommodation in the northern Malawi Rift. *Tectonophysics*, *722*, 53–68. https://doi.org/10.1016/J.TECTO.2017.10.010

Delvaux, D., & Sperner, B. (2003). Stress tensor inversion from fault kinematic indicators and focal mechanism data: The TENSOR program. In D. Nieuwland (Ed.) *New Insights into Structural Interpretation and Modelling* (Vol. 212, pp. 5–100). Geological Society, London, Special Publications. https://doi.org/10.1144/gsl.sp.2003.212.01.06

Di Naccio, D., Boncio, P., Brozzetti, F., Pazzaglia, F. J., & Lavecchia, G. (2013). Morphotectonic analysis of the Lunigiana and Garfagnana grabens (northern Apennines, Italy): Implications for active normal faulting. *Geomorphology*, *201*, 293–311. https://doi.org/10.1016/j.geomorph.2013.07.003

DISS Working Group. (2021). Database of individual seismogenic sources (DISS), version 3.3.0: A compilation of potential sources for earthquakes larger than M 5.5 in Italy and surrounding areas [Dataset]. *Istituto Nazionale di Geofisica e Vulcanologia (INGV)*. https://doi.org/10.13127/diss3.3.0

Di Stefano, R., Bianchi, I., Ciaccio, M. G., Carrara, G., & Kissling, E. (2011). Three-dimensional Moho topography in Italy: New constraints from receiver functions and controlled source seismology. *Geochemistry, Geophysics, Geosystems*, *12*(9). https://doi.org/10.1029/2011GC003649

Di Stefano, R., & Ciaccio, M. G. (2014). The lithosphere and asthenosphere system in Italy as inferred from the Vp and vs 3D velocity model and Moho map. *Journal of Geodynamics*, *82*, 16–25. https://doi.org/10.1016/j.jog.2014.09.006

Di Stefano, R., Kissling, E., Chiarabba, C., Amato, A., & Giardini, D. (2009). Shallow subduction beneath Italy: Three-dimensional images of the Adriatic-European-Tyrrhenian lithosphere system based on high-quality P wave arrival times. *Journal of Geophysical Research*, *114*(B5). https://doi.org/10.1029/2008JB005641

Doglioni, C. (1991). A proposal for the kinematic modelling of W-dipping subductions—Possible applications to the Tyrrhenian-Apennines system. *Terra Nova*, *3*(4), 423–434. https://doi.org/10.1111/j.1365-3121.1991.tb00172.x

Doglioni, C., Dagostino, N., & Mariotti, G. (1998). Normal faulting vs regional subsidence and sedimentation rate. *Marine and Petroleum Geology*, *15*(8), 737–750. https://doi.org/10.1016/S0264-8172(98)00052-X

Dramis, F., Pambianchi, G., Nesci, O., & Consoli, M. (1991). *Il ruolo di elementi strutturali trasversali nell'evoluzione tettonico-sedimentaria e geomorfologica della regione marchigiana* (pp. 287–293). Studi Geologici Camerti. Nuova serie. Retrieved from https://hdl.handle.net/11581/242451

Eagles, G., Pérez-Díaz, L., & Scarselli, N. (2015). Getting over continent ocean boundaries. *Earth-Science Reviews*, *151*, 244–265. https://doi.org/10.1016/j.earscirev.2015.10.009

Elter, F. M., Elter, P., Eva, C., Eva, E., Kraus, R. K., Padovano, M., & Solarino, S. (2012). An alternative model for the recent evolution of the Northern–Central Apennines (Italy). *Journal of Geodynamics*, *54*, 55–63. https://doi.org/10.1016/J.JOG.2011.11.001

Elter, P. (1975). Introduction a la geologie de l'Apennin septentrional. *Bulletin de la Societe Geologique de France*, *S7-XVII*(6), 956–962. https://doi.org/10.2113/gssgfbull.S7-XVII.6.956

Eva, E., Molli, G., Pettenati, F., & Solarino, S. (2025). Seismicity, seismotectonics and historical earthquakes of the northwestern Apennines, Italy: A reappraisal. *Tectonophysics*, *898*, 230642. https://doi.org/10.1016/j.tecto.2025.230642

Eva, E., Solarino, S., & Boncio, P. (2014). HypoDD relocated seismicity in northern Apennines (Italy) preceding the 2013 seismic unrest: Seismotectonic implications for the Lunigiana-Garfagnana area. *Bollettino di Geofisica Teorica ed Applicata*, *55*(4), 739–754. https://doi.org/10.4430/bgta0131

Faccenna, C., Becker, T. W., Auer, L., Billi, A., Boschi, L., Brun, J. P., et al. (2014). Mantle dynamics in the mediterranean. *Reviews of Geophysics*, *52*(3), 283–332. https://doi.org/10.1002/2013RG000444

Faccenna, C., Nalpas, T., Brun, J. P., Davy, P., & Bosi, V. (1995). The influence of pre-existing thrust faults on normal fault geometry in nature and in experiments. *Journal of Structural Geology*, *17*(8), 1139–1149. https://doi.org/10.1016/0191-8141(95)00008-2

Fazzuoli, M., Pandeli, E., & Sani, F. (1994). Considerations on the sedimentary and structural evolution of the tuscan domain since early liassic to tortonian. *Memorie Società Geologica Italiana*, *48*, 31–50. [Google Scholar].

Ferretti, G., Solarino, S., & Eva, E. (2002). Crustal structure of the Lunigiana-Garfagnana area (Tuscany, Italy): Seismicity, fault-plane solutions, and seismic tomography. *Bollettino di Geofisica Teorica ed Applicata*, *43*(3), 221–238.https://www.earth-prints.org/handle/2122/10950

Fossen, H., & Rotevatn, A. (2016). Fault linkage and relay structures in extensional settings—A review. *Earth-Science Reviews*, *154*, 14–28. https://doi.org/10.1016/J.EARSCIREV.2015.11.014

Frepoli, A., & Amato, A. (1997). Contemporaneous extension and compression in the Northern Apennines from earthquake fault-plane solutions. *Geophysical Journal International*, *129*(2), 368–388. https://doi.org/10.1111/J.1365-246X.1997.TB01589.X

Gawthorpe, R. L., & Leeder, M. R. (2000). Tectono-sedimentary evolution of active extensional basins. *Basin Research*, *12*(3-4), 195–218. https://doi.org/10.1111/j.1365-2117.2000.00121.x

Ghelardoni, R. (1965). Osservazioni sulla tettonica trasversale nell'Appennino Settentrionale. *Bollettino Società Geologica Italiana*, *84*(3), 277–290. [Google Scholar].

Ghisetti, F., & Vezzani, L. (2002). Normal faulting, extension and uplift in the outer thrust belt of the central Apennines (Italy): Role of the Caramanico fault. *Basin Research*, *14*(2), 225–236. https://doi.org/10.1046/j.1365-2117.2002.00171.x

Gola, G., Bertini, G., Bonini, M., Botteghi, S., Brogi, A., De Franco, R., et al. (2017). Data integration and conceptual modelling of the Larderello geothermal area, Italy. *Energy Procedia*, *125*, 300–309. https://doi.org/10.1016/j.egypro.2017.08.201

Green, R. G., White, R. S., & Greenfield, T. (2014). Motion in the north Iceland volcanic rift zone accommodated by bookshelf faulting. *Nature Geoscience*, *7*(1), 29–33. https://doi.org/10.1038/ngeo2012

Hanks, T. C. (1977). Earthquake stress drops, ambient tectonic stresses and stresses that drive plate motions. *Stress in the Earth*, 441–458. https://doi.org/10.1007/978-3-0348-5745-1_28

Hanks, T. C., & Kanamori, H. (1979). A moment magnitude scale. *Journal of Geophysical Research*, *84*(B5), 2348–2350. https://doi.org/10.1029/JB084iB05p02348

Harris, R. A. (1998). Introduction to special section: Stress triggers, stress shadows, and implications for seismic hazard. *Journal of Geophysical Research*, *103*(B10), 24347–24358. https://doi.org/10.1029/98JB01576

Homberg, C., Bergerat, F., Philippe, Y., Lacombe, O., & Angelier, J. (2002). Structural inheritance and Cenozoic stress fields in the Jura fold-and-thrust belt (France). *Tectonophysics*, *357*(1–4), 137–158. https://doi.org/10.1016/S0040-1951(02)00366-9

Illsley-Kemp, F., Bull, J. M., Keir, D., Gerya, T., Pagli, C., Gernon, T., et al. (2018). Initiation of a proto-transform fault prior to seafloor spreading. *Geochemistry, Geophysics, Geosystems*, *19*(12), 4744–4756. https://doi.org/10.1029/2018gc007947

Illies, J. H. (1972). The Rhine graben rift system-plate tectonics and transform faulting. *Geophysical Surveys*, *1*(1), 27–60. https://doi.org/10.1007/BF01449550

ISIDe Working Group. (2007). Italian seismological instrumental and parametric database (ISIDe) (version 1) [Dataset]. *Istituto Nazionale di Geofisica e Vulcanologia (INGV)*. https://doi.org/10.13127/ISIDE

Istituto Nazionale di Geofisica e Vulcanologia (INGV). (2005). Rete sismica Nazionale (RSN) [Dataset]. *Istituto Nazionale di Geofisica e Vulcanologia (INGV)*. https://doi.org/10.13127/sd/x0fxnh7qfy

ITHACA Working Group. (2019). ITHACA (Italy HAzard from CApable faulting), A database of active capable faults of the Italian territory. Version December 2019. *ISPRA Geological Survey of Italy*. Retrieved from https://sgi.isprambiente.it/ithacaweb/default.aspx#1

Jiménez-Bonilla, A., Crespo-Blanc, A., Balanyá, J. C., Expósito, I., & Díaz-Azpiroz, M. (2020). Analog models of fold-and-thrust wedges in progressive arcs: A comparison with the Gibraltar arc external wedge. *Frontiers in Earth Science*, *8*, 72. https://doi.org/10.3389/feart.2020.00072

Jolivet, L., & Faccenna, C. (2000). Mediterranean extension and the Africa-Eurasia collision. *Tectonics*, *19*(6), 1095–1106. https://doi.org/10.1029/2000TC900018

Jolivet, L., Faccenna, C., Goffé, B., Mattei, M., Rossetti, F., Brunet, C., et al. (1998). Midcrustal shear zones in postorogenic extension: Example from the northern Tyrrhenian Sea. *Journal of Geophysical Research*, *103*(6), 12123–12160. https://doi.org/10.1029/97jb03616

Kaerger, L., Del Ventisette, C., Vannucchi, P., Molli, G., Pagli, C., & Keir, D. (2024). Relocation of earthquake clusters show seismogenic transverse structures in the Inner Northern Apennines (Italy). *Frontiers in Earth Science*, *12*, 1474036. https://doi.org/10.3389/feart.2024.1474036

Kastens, K. A., & Mascle, J. (1990). The geological evolution of the Tyrrhenian Sea: An introduction to the scientific results of ODP Leg 107. In *Proceedings of the ocean drilling program, scientific results* (Vol. 107). https://doi.org/10.2973/odp.proc.sr.107.187.1990

King, G. C. P., Stein, R. S., & Lin, J. (1994). Static stress changes and the triggering of earthquakes. *Bulletin of the Seismological Society of America*, *84*(3), 935–953. https://doi.org/10.1785/BSSA0840030935

Laõ-Dávila, D. A., Al-Salmi, H. S., Abdelsalam, M. G., & Atekwana, E. A. (2015). Hierarchical segmentation of the Malawi Rift: The influence of inherited lithospheric heterogeneity and kinematics in the evolution of continental rifts. *Tectonics*, *34*(12), 2399–2417. https://doi.org/10.1002/2015TC003953

La Rosa, A., Pagli, C., Hurman, G. L., & Keir, D. (2022). Strain accommodation by intrusion and faulting in a rift linkage zone: Evidences from high-resolution topography data of the afrera plain (Afar, east Africa). *Tectonics*, *41*(6), e2021TC007115. https://doi.org/10.1029/2021TC007115

La Rosa, A., Pagli, C., Molli, G., Casu, F., De Luca, C., Pieroni, A., & D'Amato Avanzi, G. (2018). Growth of a sinkhole in a seismic zone of the northern Apennines (Italy). *Natural Hazards and Earth System Sciences*, *18*(9), 2355–2366. https://doi.org/10.5194/nhess-18-2355-2018

Latorre, D., Di Stefano, R., Castello, B., Michele, M., & Chiaraluce, L. (2023). An updated view of the Italian seismicity from probabilistic location in 3D velocity models: The 1981–2018 Italian catalog of absolute earthquake locations (CLASS). *Tectonophysics*, *846*, 229664. https://doi.org/10.1016/j.tecto.2022.229664

Le Breton, E., Handy, M. R., Molli, G., & Ustaszewski, K. (2017). Post-20 Ma motion of the Adriatic plate: New constraints from surrounding orogens and implications for crust-mantle decoupling. *Tectonics*, *36*(12), 3135–3154. https://doi.org/10.1002/2016TC004443

Lezzar, K. E., Tiercelin, J.-J., Le Turdu, C., Cohen, A. S., Reynolds, D. J., Le Gall, B., & Scholz, C. A. (2002). Control of normal fault interaction on the distribution of major Neogene sedimentary depocenters, lake Tanganyika, east African rift. *AAPG Bulletin*, *86*(6), 1027–1059. https://doi.org/10.1306/61EEDC1A-173E-11D7-8645000102C1865D

Li, H., Michelini, A., Zhu, L., Bernardi, F., & Spada, M. (2007). Crustal velocity structure in Italy from analysis of regional seismic waveforms. *Bulletin of the Seismological Society of America*, *97*(6), 2024–2039. https://doi.org/10.1785/0120070071

Lin, J., & Stein, R. S. (2004). Stress triggering in thrust and subduction earthquakes and stress interaction between the southern San Andreas and nearby thrust and strike-slip faults. *Journal of Geophysical Research*, *109*(B2). https://doi.org/10.1029/2003JB002607

Liotta, D. (1991). The arbia-val marecchia line, northern Apennines. *Eclogae Geologicae Helvetiae*, *84*(2), 413–430. [Google Scholar].

Liotta, D., & Brogi, A. (2020). Pliocene-Quaternary fault kinematics in the Larderello geothermal area (Italy): Insights for the interpretation of the present stress field. *Geothermics*, *83*, 101714. https://doi.org/10.1016/j.geothermics.2019.101714

Liotta, D., Brogi, A., Meccheri, M., Dini, A., Bianco, C., & Ruggieri, G. (2015). Coexistence of low-angle normal and high-angle strike-to oblique-slip faults during Late Miocene mineralization in eastern Elba Island (Italy). *Tectonophysics*, *660*, 17–34. https://doi.org/10.1016/j.tecto.2015.06.025

Locardi, E. (1988). The origin of the Apenninic arcs. *Tectonophysics*, *146*(1), 105–123. https://doi.org/10.1016/0040-1951(88)90085-6

Locati, M., Camassi, R., Rovida, A., Ercolani, E., Bernardini, F., Castelli, V., et al. (2022). Database macrosismico italiano (DBMI15), versione 4.0 [Dataset]. *Istituto Nazionale di Geofisica e Vulcanologia (INGV)*. https://doi.org/10.13127/dbmi/dbmi15.4

Lomax, A., Michelini, A., & Curtis, A. (2014). Earthquake location, direct, global-search methods [software], In *Encyclopedia of complexity and systems science*. R. Meyers (Ed.). Springer. https://doi.org/10.1007/978-3-642-27737-5_150-2

Lomax, A., Virieux, J., Volant, P., & Berge-Thierry, C. (2000). Probabilistic earthquake location in 3D and layered models [software], In *Advances in seismic event location*. C. H. Thurber, & N. Rabinowitz (Eds.), Vol. *18*, (pp. 101–134). *Modern Approaches in Geophysics*. https://doi.org/10.1007/978-94-015-9536-0_5

Macdonald, K. C., Fox, P. J., Perram, L. J., Eisen, M. F., Haymon, R. M., Miller, S. P., et al. (1988). A new view of the mid-ocean ridge from the behaviour of ridge-axis discontinuities. *Nature*, *335*(6187), 217–225. https://doi.org/10.1038/335217a0

Maestrelli, D., Montanari, D., Corti, G., Ventisette, C. D., Moratti, G., & Bonini, M. (2020). Exploring the interactions between rift propagation and inherited crustal fabrics through experimental modeling. *Tectonics*, *39*(12), e2020TC006211. https://doi.org/10.1029/2020TC006211

Mantovani, E., Viti, M., Cenni, N., Babbucci, D., & Tamburelli, C. (2015). Present velocity field in the Italian region by GPS data: Geodynamic/tectonic implications. *International Journal of Geosciences*, *6*(12), 1285–1316. https://doi.org/10.4236/IJG.2015.612103

Mariotti, G., & Doglioni, C. (2000). The dip of the foreland monocline in the Alps and Apennines. *Earth and Planetary Science Letters*, *181*(1–2), 191–202. https://doi.org/10.1016/S0012-821X(00)00192-8

Mariucci, M. T., & Montone, P. (2024). *IPSI 1.6, database of Italian present-day stress indicators*. Istituto Nazionale di Geofisica e Vulcanologia (INGV). https://doi.org/10.13127/IPSI.1.6

Martelli, L., Bonini, M., Calabrese, L., Corti, G., Ercolessi, G., Molinari, F. C., et al. (2016a). *Note illustrative della carta sismotettonica della Regione Emilia Romagna ed aree limitrofe*. Regione Emilia-Romagna, Servizio Geologico, Sismico e dei Suoli, D.R.E.AM. Italia Ed. Retrieved from https://hdl.handle.net/2158/1105719

Martelli, L., Bonini, M., Calabrese, L., Corti, G., Ercolessi, G., Molinari, F. C., et al. (2016b). *Carta sismotettonica della Regione Emilia Romagna ed aree limitrofe*. Regione Emilia-Romagna, Servizio Geologico, Sismico e dei Suoli, D.R.E.AM. Italia Ed.

Martin, M. W., Glazner, A. F., Walker, J. D., & Schermer, E. R. (1993). Evidence for right-lateral transfer faulting accommodating en echelon Miocene extension, Mojave Desert, California. *Geology*, *21*, 355–358. https://doi.org/10.1130/0091-7613(1993)021<0355:EFRLTF>2.3.CO;2

Mazzoli, S., Macchiavelli, C., & Ascione, A. (2014). The 2013 marche offshore earthquakes: New insights into the active tectonic setting of the outer northern Apennines. *Journal of the Geological Society*, *171*(4), 457–460. https://doi.org/10.1144/jgs2013-091

McClay, K., & Khalil, S. (1998). Extensional hard linkages, eastern Gulf of Suez, Egypt. *Geology*, *26*(6), 563–566. https://doi.org/10.1130/0091-7613(1998)026<0563:ehlego>2.3.co;2

McClay, K. R. (1995). The geometries and kinematics of inverted fault systems: A review of analogue model studies. *Geological Society, London, Special Publications*, *88*, 97–118. https://doi.org/10.1144/GSL.SP.1995.088.01.07

Mele, G., & Sandvol, E. (2003). Deep crustal roots beneath the northern Apennines inferred from teleseismic receiver functions. *Earth and Planetary Science Letters*, *211*(1), 69–78. https://doi.org/10.1016/S0012-821X(03)00185-7

Meletti, C., Galadini, F., Valensise, G., Stucchi, M., Basili, R., Barba, S., et al. (2008). A seismic source zone model for the seismic hazard assessment of the Italian territory. *Tectonophysics*, *450*(1), 85–108. https://doi.org/10.1016/j.tecto.2008.01.003

Meletti, C., Patacca, E., & Scandone, P. (2000). Construction of a seismotectonic model: The case of Italy. *Pure and Applied Geophysics*, *157*(1), 11–35. https://doi.org/10.1007/PL00001089

Michele, M., Latorre, D., & Emolo, A. (2019). An empirical formula to classify the quality of earthquake locations. *Bulletin of the Seismological Society of America*, *109*(6), 2755–2761. https://doi.org/10.1785/0120190144

Milia, A., & Torrente, M. M. (2015). Tectono-stratigraphic signature of a rapid multistage subsiding rift basin in the tyrrhenian-apennine hinge zone (Italy): A possible interaction of upper plate with subducting slab. *Journal of Geodynamics*, *86*, 42–60. https://doi.org/10.1016/j.jog.2015.02.005

Mirabella, F., Braun, T., Brogi, A., & Capezzuoli, E. (2022). Pliocene–Quaternary seismogenic faults in the inner Northern Apennines (Valdelsa Basin, southern Tuscany) and their role in controlling the local seismicity. *Geological Magazine*, *159*(6), 853–872. https://doi.org/10.1017/S0016756822000036

Molli, G. (2008). Northern Apennine-Corsica orogenic system: An updated overview. *Geological Society Special Publication*, *298*(1), 413–442. https://doi.org/10.1144/SP298.19

Molli, G., Carlini, M., Vescovi, P., Artoni, A., Balsamo, F., Camurri, F., et al. (2018). Neogene 3-D structural architecture of The North-west Apennines: The role of the low-angle normal faults and basement thrusts. *Tectonics*, *37*(7), 2165–2196. https://doi.org/10.1029/2018TC005057

Molli, G., Doveri, M., Manzella, A., Bonini, L., Botti, F., Menichini, M., et al. (2015). Surface-subsurface structural architecture and groundwater flow of the Equi Terme hydrothermal area, northern Tuscany Italy. *Italian Journal of Geosciences*, *134*(3), 442–457. https://doi.org/10.3301/IJG.2014.25

Molli, G., Manighetti, I., Bennett, R., Malavieille, J., Serpelloni, E., Storti, F., et al. (2021). Active fault systems in the inner northwest Apennines, Italy: A reappraisal one century after the 1920 Mw∼ 6.5 Fivizzano earthquake. *Geosciences*, *11*(3), 139. https://doi.org/10.3390/geosciences11030139

Molli, G., Torelli, L., & Storti, F. (2016). The 2013 Lunigiana (Central Italy) earthquake: Seismic source analysis from DInSar and seismological data, and geodynamic implications for the northern Apennines. A discussion. *Tectonophysics*, *668*, 108–112. https://doi.org/10.1016/j.tecto.2015.07.041

Montone, P., & Mariucci, M. T. (2016). The new release of the Italian contemporary stress map. *Geophysical Journal International*, *205*(3), 1525–1531. https://doi.org/10.1093/gji/ggw100

Morley, C. K. (2010). Stress re-orientation along zones of weak fabrics in rifts: An explanation for pure extension in "oblique" rift segments? *Earth and Planetary Science Letters*, *297*(3–4), 667–673. https://doi.org/10.1016/J.EPSL.2010.07.022

Morley, C. K. (2017). The impact of multiple extension events, stress rotation and inherited fabrics on normal fault geometries and evolution in the Cenozoic rift basins of Thailand. *Geological Society, London, Special Publications*, *439*(1), 413–445. https://doi.org/10.1144/SP439.3

Morley, C. K., Gabdi, S., & Seusutthiya, K. (2007). Fault superimposition and linkage resulting from stress changes during rifting: Examples from 3D seismic data, Phitsanulok Basin, Thailand. *Journal of Structural Geology*, *29*(4), 646–663. https://doi.org/10.1016/j.jsg.2006.11.005

Muirhead, J. D., & Kattenhorn, S. A. (2018). Activation of preexisting transverse structures in an evolving magmatic rift in East Africa. *Journal of Structural Geology*, *106*, 1–18. https://doi.org/10.1016/J.JSG.2017.11.004

Nguyen, L. C., Hall, S. A., Bird, D. E., & Ball, P. J. (2016). Reconstruction of the east Africa and Antarctica continental margins. *Journal of Geophysical Research: Solid Earth*, *121*(6), 4156–4179. https://doi.org/10.1002/2015JB012776

Nirta, G., Principi, G., & Vannucchi, P. (2007). The Ligurian units of western Tuscany (northern Apennines): Insight on the influence of pre-existing weakness zones during ocean closure. *Geodinamica Acta*, *20*(1–2), 71–97. https://doi.org/10.3166/ga.20.71-97

Okada, Y. (1992). Internal deformation due to shear and tensile faults in a half-space. *Bulletin of the Seismological Society of America*, *82*(2), 1018–1040. https://doi.org/10.1785/BSSA0820021018

Ottria, G., & Molli, G. (2000). Superimposed brittle structures in the late-orogenic extension of the northern Apennine: Results from the Carrara area (Alpi Apuane, NW Tuscany). *Terra Nova*, *12*(2), 52–59. https://doi.org/10.1111/j.1365-3121.2000.00272.x

Pace, B., Boncio, P., & Lavecchia, G. (2002). The 1984 Abruzzo earthquake (Italy): An example of seismogenic process controlled by interaction between differently oriented synkinematic faults. *Tectonophysics*, *350*(3), 237–254. https://doi.org/10.1016/S0040-1951(02)00118-X

Paige, C. C., & Saunders, M. A. (1982). LSQR: An algorithm for sparse linear Equations and sparse least squares. *ACM Transactions on Mathematical Software*, *8*(1), 43–71. https://doi.org/10.1145/355984.355989

Pascucci, V., Costantini, A., Martini, I. P., & Dringoli, R. (2006). Tectono-sedimentary analysis of a complex, extensional, Neogene basin formed on thrust-faulted, Northern Apennines hinterland: Radicofani Basin, Italy. *Sedimentary Geology*, *183*(1), 71–97. https://doi.org/10.1016/j.sedgeo.2005.09.009

Pascucci, V., Martini, I. P., Sagri, M., & Sandrelli, F. (2007). Effects of transverse structural lineaments on the Neogene–quaternary basins of Tuscany (inner northern Apennines, Italy). *Sedimentary processes, environments and basins: a tribute to Peter Friend*, 155–182. https://doi.org/10.1002/9781444304411.ch8

Pezzo, G., Boncori, J. P. M., Atzori, S., Piccinini, D., Antonioli, A., & Salvi, S. (2014). The 2013 Lunigiana (Central Italy) earthquake: Seismic source analysis from DInSAR and seismological data, and geodynamical implications for the northern Apennines. *Tectonophysics*, *636*, 315–324. https://doi.org/10.1016/j.tecto.2014.09.005

Piana Agostinetti, N., & Amato, A. (2009). Moho depth and V/V ratio in peninsular Italy from teleseismic receiver functions. *Journal of Geophysical Research*, *114*(B6). https://doi.org/10.1029/2008JB005899

Picotti, V., & Pazzaglia, F. J. (2008). A new active tectonic model for the construction of the Northern Apennines mountain front near Bologna (Italy). *Journal of Geophysical Research*, *113*(B8). https://doi.org/10.1029/2007JB005307

Pizzi, A., Di Domenica, A., Gallovič, F., Luzi, L., & Puglia, R. (2017). Fault segmentation as constraint to the occurrence of the main shocks of the 2016 Central Italy seismic sequence. *Tectonics*, *36*(11), 2370–2387. https://doi.org/10.1002/2017TC004652

Pizzi, A., & Galadini, F. (2009). Pre-existing cross-structures and active fault segmentation in the northern-central Apennines (Italy). *Tectonophysics*, *476*(1), 304–319. https://doi.org/10.1016/j.tecto.2009.03.018

Plesi, G., Bonanni, G., Botti, F., Daniele, G., & Palandri, S. (1998). Processi e tempi di costruzione della catena appenninica nelle sue fasi oligo-mioceniche; l'esempio della finestra di Pracchiola (biostratigrafia, petrografia e analisi strutturale, con carta geologico-strutturale scala 1: 20,000). *Italian Journal of Geosciences*, *117*(3), 841–894. [Google Scholar].

Plesi, G., Daniele, G., Chicchi, S., Bettelli, G., Catanzariti, R., Cerrina Feroni, A., et al. (2002a). *Note illustrative alla Carta Geologica d'Italia alla scala 1:50.000. Foglio 235 "Pievepelago"*. Regione Emilia Romagna. S.EL.CA. Firenze. [Google Scholar].

Plesi, G., Daniele, G., Chicchi, S., Bettelli, G., Catanzariti, R., Cerrina Feroni, A., et al. (2002b). *Carta geologica d'Italia alla scala 1:50.000. Foglio 235 "Pievepelago"*. Regione Emilia Romagna. S.EL.CA. Firenze. [Google Scholar].

Pondrelli, S., Salimbeni, S., Ekström, G., Morelli, A., Gasperini, P., & Vannucci, G. (2006). The Italian CMT dataset from 1977 to the present. *Physics of the Earth and Planetary Interiors*, *159*(3), 286–303. https://doi.org/10.1016/j.pepi.2006.07.008

Puccinelli, A. (1987). Un esempio di tettonica recente nella Val di Serchio: Il sollevamento di Monte Perpoli. *Atti Della Società Toscana Di Scienze Naturali Memorie Serie A*, *94*, 105–117. [Google Scholar].

Puccinelli, A., D'Amato Avanzi, G., Perilli, N., Carmignani, L., Meccheri, M., Conti, P., et al. (2016a). *Note illustrative alla Carta geologica d'Italia alla scala 1:50.000. Foglio 250 "Castelnuovo Garfagnana"*. Dipartimento di Scienze della Terra, Università di Pisa. Retrieved from https://www.isprambiente.gov.it/Media/carg/note_illustrative/250_Castelnuovo_Garfagnana.pdf

Puccinelli, A., D'Amato Avanzi, G., Perilli, N., Carmignani, L., Meccheri, M., Conti, P., et al. (2016b). Carta geologica d'Italia alla scala 1: 50.000. Foglio 250 "Castelnuovo Garfagnana". *Dipartimento di Scienze della Terra, Università di Pisa*. [Google Scholar].

Remitti, F., Bettelli, G., & Vannucchi, P. (2007). Internal structure and tectonic evolution of an underthrust tectonic mélange: The Sestola-Vidiciatico tectonic unit of the Northern Apennines, Italy. *Geodinamica Acta*, *20*(1–2), 37–51. https://doi.org/10.3166/ga.20.37-51

Reutter, K. J., Teichmüller, M., Teichmüller, R., & Zanzucchi, G. (1983). The coalification pattern in the Northern Apennines and its palaeogeothermic and tectonic significance. *Geologische Rundschau*, *72*(3), 861–893. https://doi.org/10.1007/BF01848346

Rosenbaum, G., Gasparon, M., Lucente, F. P., Peccerillo, A., & Miller, M. S. (2008). Kinematics of slab tear faults during subduction segmentation and implications for Italian magmatism. *Tectonics*, *27*(2). https://doi.org/10.1029/2007TC002143

Rosenbaum, G., & Piana Agostinetti, N. (2015). Crustal and upper mantle responses to lithospheric segmentation in the northern Apennines. *Tectonics*, *34*(4), 648–661. https://doi.org/10.1002/2013TC003498

Rovida, A., Locati, M., Camassi, R., Lolli, B., Gasperini, P., & Antonucci, A. (2022). Italian parametric earthquake catalogue (CPTI15), version 4.0 [Dataset]. *Istituto Nazionale di Geofisica e Vulcanologia (INGV)*. https://doi.org/10.13127/cpti/cpti15.4

Saccorotti, G., Bruni, R., Bonini, M., Corti, G., Keir, D., & Sani, F. (2022). Recent seismic sequences and activation of normal fault systems in the Mugello basin and surrounding areas (northern Apennines, Italy). *Frontiers in Earth Science*, *10*, 879160. https://doi.org/10.3389/feart.2022.879160

Savelli, C., & Ligi, M. (2017). An updated reconstruction of basaltic crust emplacement in Tyrrhenian sea, Italy. *Scientific Reports*, *7*(1), 18024. https://doi.org/10.1038/s41598-017-17625-2

Scholz, C. H. (2002). *The mechanics of earthquakes and faulting* (2nd ed.). Cambridge University Press. https://doi.org/10.1017/CBO9780511818516

Scognamiglio, L., Tinti, E., & Quintiliani, M. (2006). Time domain moment tensor (TDMT) [Dataset]. *Istituto Nazionale di Geofisica e Vulcanologia (INGV)*. https://doi.org/10.13127/TDMT

Scudero, S., Marcocci, C., & D'Alessandro, A. (2021). Insights on the Italian seismic network from location uncertainties. *Journal of Seismology*, *25*(4), 1061–1076. https://doi.org/10.1007/s10950-021-10011-6

Serpelloni, E., Anzidei, M., Baldi, P., Casula, G., & Galvani, A. (2005). Crustal velocity and strain-rate fields in Italy and surrounding regions: New results from the analysis of permanent and non-permanent GPS networks. *Geophysical Journal International*, *161*(3), 861–880. https://doi.org/10.1111/j.1365-246X.2005.02618.x

Serpelloni, E., Cavaliere, A., Martelli, L., Pintori, F., Anderlini, L., Borghi, A., et al. (2022). Surface velocities and strain-rates in the euro-mediterranean region from massive GPS data processing. *Frontiers in Earth Science*, *10*, 907897. https://doi.org/10.3389/FEART.2022.907897/BIBTEX

Serpelloni, E., Vannucci, G., Anderlini, L., & Bennett, R. A. (2016). Kinematics, seismotectonics and seismic potential of the eastern sector of the European Alps from GPS and seismic deformation data. *Tectonophysics*, *688*, 157–181. https://doi.org/10.1016/j.tecto.2016.09.026

Sibson, R. H. (1974). Frictional constraints on thrust, wrench and normal faults. *Nature*, *249*(5457), 542–544. https://doi.org/10.1038/249542a0

Snoke, J. (2003). 85.12 FOCMEC: FOCal MEChanism determinations. *International Geophysics*, *81*, 1629–1630. https://doi.org/10.1016/S0074-6142(03)80291-7

Snoke, J. A., Munsey, J. W., Teague, A. G., & Bollinger, G. A. (1984). A program for focal mechanism determination by combined use of polarity and SV-P amplitude ratio data. *Earthquake Notes*, *55*. [Google Scholar].

Sorgi, C., Deffontaines, B., Hippolyte, J. C., & Cadet, J. P. (1998). An integrated analysis of transverse structures in the northern Apennines, Italy. *Geomorphology*, *25*(3–4), 193–206. https://doi.org/10.1016/S0169-555X(98)00041-5

Stein, R. S. (1999). The role of stress transfer in earthquake occurrence. *Nature*, *402*(6762), 605–609. https://doi.org/10.1038/45144

Storti, F., Salvini, F., Rossetti, F., & Morgan, J. P. (2007). Intraplate termination of transform faulting within the Antarctic continent. *Earth and Planetary Science Letters*, *260*(1–2), 115–126. https://doi.org/10.1016/j.epsl.2007.05.020

Stramondo, S., Vannoli, P., Cannelli, V., Polcari, M., Melini, D., Samsonov, S., et al. (2014). X- and C-band SAR surface displacement for the 2013 Lunigiana earthquake (northern Italy): A Breached relay ramp? *Ieee Journal of Selected Topics in Applied Earth Observations and Remote Sensing*, *7*(7), 2746–2753. https://doi.org/10.1109/JSTARS.2014.2313640

Tarantola, A., & Valette, B. (1982). Generalized nonlinear inverse problems solved using the least squares criterion. *Reviews of Geophysics*, *20*(2), 219–232. https://doi.org/10.1029/RG020i002p00219

Tavani, S., Cardello, G. L., Vignaroli, G., Balsamo, F., Parente, M., Sabbatino, M., et al. (2021). Segmentation of the Apenninic margin of the Tyrrhenian back-Arc basin forced by the subduction of an inherited transform system. *Tectonics*, *40*(9), e2021TC006770. https://doi.org/10.1029/2021TC006770

Tavani, S., Granado, P., Corradetti, A., Seers, T., Casas, J. M., & Muñoz, J. A. (2020). Transverse jointing in foreland fold-and-thrust belts: A remote sensing analysis in the eastern Pyrenees. *Solid Earth*, *11*(5), 1643–1651. https://doi.org/10.5194/se-11-1643-2020

Tavarnelli, E., Butler, R. W. H., Decandia, F. A., Calamita, F., Grasso, M., Alvarez, W., & D'offizi, S. (2004). Implications of fault reactivation and structural inheritance in the Cenozoic tectonic evolution of Italy. *The geology of Italy, special*, *1*, 209–222. [Google Scholar].

Tavarnelli, E., Decandia, F. A., Renda, P., Tramutoli, M., Gueguen, E., & Alberti, M. (2001). Repeated reactivation in the Apennine-Maghrebide system, Italy: A possible example of fault-zone weakening? In *Geological Society, London, Special Publications*, R. E. Holdsworth, R. A. Strachan, J. F. Magloughlin, & R. J. Knipe (Eds.), Vol. 186(1), (pp. 273–286). *The nature and tectonic significance of fault zone weakening*. https://doi.org/10.1144/GSL.SP.2001.186.01.16

Taylor, B., Goodliffe, A., & Martinez, F. (2009). Initiation of transform faults at rifted continental margins. *Comptes Rendus Geoscience*, *341*(5), 428–438. https://doi.org/10.1016/j.crte.2008.08.010

Tian, D., Uieda, L., Leong, W. J., Fröhlich, Y., Schlitzer, W., Grund, M., et al. (2024). PyGMT: A Python interface for the generic mapping Tools (v0.14.0) [Software]. *Zenodo*. https://doi.org/10.5281/zenodo.14535921

Toda, S., Stein, R. S., Richards-Dinger, K., & Bozkurt, S. B. (2005). Forecasting the evolution of seismicity in southern California: Animations built on earthquake stress transfer. *Journal of Geophysical Research*, *110*(B5). https://doi.org/10.1029/2004JB003415

Toda, S., Stein, R. S., Sevilgen, V., & Lin, J. (2011). Coulomb 3.3 Graphic-rich deformation and stress-change software for earthquake, tectonic, and volcano research and teaching-user guide [Software]. *U.S. Geological Survey Open-File Report 2011–1060*, *63*. Retrieved from https://pubs.usgs.gov/of/2011/1060/

Tyler, S., Bull, J. M., Parson, L. M., & Tuckwell, G. W. (2007). Numerical modelling of non-transform discontinuity geometry: Implications for ridge structure, volcano-tectonic fabric development and hydrothermal activity at segment ends. *Earth and Planetary Science Letters*, *257*(1–2), 146–159. https://doi.org/10.1016/j.epsl.2007.02.028

Vannoli, P., Bernardi, F., Palombo, B., Vannucci, G., Console, R., & Ferrari, G. (2016). New constraints shed light on strike-slip faulting beneath the southern Apennines (Italy): The 21 August 1962 Irpinia multiple earthquake. *Tectonophysics*, *691*, 375–384. https://doi.org/10.1016/j.tecto.2016.10.032

Vannoli, P., Burrato, P., & Valensise, G. (2015). The seismotectonics of the Po Plain (northern Italy): Tectonic diversity in a blind faulting domain. *Pure and Applied Geophysics*, *172*(5), 1105–1142. https://doi.org/10.1007/s00024-014-0873-0

Vannucchi, P., Remitti, F., & Bettelli, G. (2008). Geologic record of fluid flow and seismogenesis along an erosive subducting plate boundary. *Nature*, *451*(7179), 699–703. https://doi.org/10.1038/nature06486

Vannucchi, P., Remitti, F., & Bettelli, G. (2012). Lateral variability of the erosive plate boundary in the Northern Apennines, Italy. *Italian Journal of Geosciences*, *131*(2), 215–227. https://doi.org/10.3301/IJG.2012.11

Vaselli, L., Berretti, G., & Molli, G. (2008). *Deformazione fragile delle Alpi Apuane Centro-orientali: Risultati preliminari* (Vol. 186). Rendiconti Online. [Google Scholar].

Vescovi, P. (2005). The middle Miocene Mt. Ventasso-Mt. Cimone arcuate structure of the Emilia Apennines. *Italian Journal of Geosciences*, *124*(1), 53–67. [Google Scholar].

Waldhauser, F. (2001). HypoDD: A computer program to compute double-difference earthquake locations [Software]. *USGS Open File Rep*, 01–113. https://doi.org/10.3133/ofr01113

Waldhauser, F., & Ellsworth, W. L. (2000). A double-difference earthquake location algorithm: Method and Application to the northern Hayward fault, California. *Bulletin of the Seismological Society of America*, *90*(6), 1353–1368. https://doi.org/10.1785/0120000006

Willemse, E. J., Peacock, D. C., & Aydin, A. (1997). Nucleation and growth of strike-slip faults in limestones from Somerset, UK. *Journal of Structural Geology*, *19*(12), 1461–1477. https://doi.org/10.1016/S0191-8141(97)00056-4

Wilson, L. F., Pazzaglia, F. J., & Anastasio, D. J. (2009). A fluvial record of active fault-propagation folding, Salsomaggiore anticline, northern Apennines, Italy. *Journal of Geophysical Research*, *114*(B8). https://doi.org/10.1029/2008JB005984

Zwaan, F., & Schreurs, G. (2017). How oblique extension and structural inheritance influence rift segment interaction: Insights from 4D analog models. *Interpretation*, *5*(1), SD119–SD138. https://doi.org/10.1190/INT-2016-0063.1

## References From the Supporting Information

Aki, K. (1965). A note on the use of microseisms in determining the shallow structures of the earth's crust. *Geophysics*, *30*(4), 665–666. https://doi.org/10.1190/1.1439640

Bender, B. (1983). Maximum likelihood estimation of b values for magnitude grouped data. *Bulletin of the Seismological Society of America*, *73*(3), 831–851. https://doi.org/10.1785/BSSA0730030831

Latorre, D., Di Stefano, R., Castello, B., Michele, M., & Chiaraluce, L. (2022). Catalogo delle Localizzazioni ASSolute (CLASS): Locations (version 1) [Dataset]. *Istituto Nazionale di Geofisica e Vulcanologia (INGV)*. https://doi.org/10.13127/class.1.0

Wiemer, S., & Wyss, M. (2000). Minimum magnitude of completeness in earthquake catalogs: Examples from Alaska, the western United States, and Japan. *Bulletin of the Seismological Society of America*, *90*(4), 859–869. https://doi.org/10.1785/0119990114